Canopy structure, topography and weather are equally important drivers of small-scale snow cover dynamics in sub-alpine forests

Giulia Mazzotti[1,2], Clare Webster[1,3], Louis Quéno[1], Bertrand Cluzet[1], Tobias Jonas[1]

[1]WSL Institute for Snow and Avalanche Research SLF, 7260 Davos Dorf, Switzerland

5 [2]Univ. Grenoble Alpes, Université de Toulouse, Météo-France, CNRS, CNRM, Centre d'Études de la Neige, 38100 St. Martin d'Hères, France

[3]Department of Geosciences, University of Oslo, 0316 Oslo, Norway

Correspondence to: Giulia Mazzotti (giulia.mazzotti@slf.ch)

Abstract. In mountain regions, forests that overlap with seasonal snow mostly reside in complex terrain. Due to persisting

10 major observational challenges in these environments, the combined impact of forest structure and topography on seasonal snow cover dynamics is still poorly understood. Recent advances in forest snow process representation and increasing availability of detailed canopy structure datasets, however, now allow for hyper-resolution (<5 m) snow model simulations capable of resolving tree-scale processes, which can shed light on the complex process interactions that govern forest snow dynamics. We present multi-year simulations at 2 m resolution obtained with FSM2, a mass- and energy-balance based

15 forest snow model specifically developed and validated for meter-scale applications. We simulate a ~ 3 km² model domain encompassing forested slopes of a sub-alpine valley in the Eastern Swiss Alps and six snow seasons. Simulations thus span a wide range of canopy structures, terrain characteristics, and meteorological conditions. We analyse spatial and temporal variations in forest snow energy balance partitioning, aiming to quantify and understand the contribution of individual energy exchange processes at different locations and times. Our results suggest that snow cover evolution is equally affected

20 by canopy structure, terrain characteristics and meteorological conditions. We show that the interaction of these three factors can lead to snow distribution and melt patterns that vary between years. We further identify higher snow distribution variability and complexity in slopes that receive solar radiation early in winter. Our process-level insights corroborate and complement existing empirical findings that are largely based on snow distribution datasets only. Hyper-resolution simulations as presented here thus help to better understand how snowpacks and ecohydrological regimes in sub-alpine

25 regions may evolve as a result of forest disturbances and a warming climate. They could further support the development of process-based sub-grid forest snow cover parametrizations or tiling approaches for coarse-resolution modelling applications.

1 Introduction

The presence of snow in the sub-alpine forest ecoregion of the European Alps, and other mountain ranges across the Northern Hemisphere, means large areas of seasonal snow cover overlap with both forests and complex topography. Snow

30 accumulation and melt processes are known to be controlled by the structure of the forest cover (Mazzotti et al., 2019a),

topographic characteristics (Broxton et al., 2020; Safa et al., 2021), as well as how these physiographic factors interact with local climate and weather patterns (Lundquist et al., 2013; Seyednasrollah and Kumar, 2019; Pflug and Lundquist, 2020). Consequently, snow cover dynamics in sub-alpine forest are subject to strong complexity and variability down to small spatial and temporal scales. A thorough understanding of the controlling factors is important because snow cover dynamics

35 affect eco-hydrological regimes (e.g. Barnhart et al., 2016; Manning et al., 2022), microclimate and habitat characteristics (e.g. Niittynen et al., 2020), as well as land surface energy exchange (e.g. Webster and Jonas, 2018; Manninen and Jääskeläinen, 2018). In view of ongoing changes in both, snow cover regimes due to increasing temperatures (Mote et al., 2018; Marty et al., 2017; Notarnicola, 2020; Bormann et al., 2018), and forest structure following manmade and natural disturbances (Bebi et al., 2017; Seidl et al., 2017; Goeking and Tarboton, 2020), it is also urgent and pertinent to adequate

40 forest and water resources management strategies - particularly in regions where downstream water supply is dependent on snow resources from forested headwaters (Sturm et al., 2017; Siirila-Woodburn et al., 2021). However, it remains unclear whether landscape heterogeneity entails a variable response of snow cover dynamics to environmental change.

Canopy structural controls on individual forest processes have been widely addressed in both experimental and modelling studies but only few studies have considered how the combination of forest and topography alter accumulation and melt

45 processes. Interception of snow by the canopy (Moeser et al., 2015; Roth and Nolin, 2019), transmission of shortwave, and enhancement of longwave radiation (Malle et al., 2019; Mazzotti et al., 2019b; Webster et al., 2016; Lawler and Link, 2011), have received particular attention due to the strong spatial variability of these processes induced by tree-scale canopy structural heterogeneity. Existing research has, however, focused on flat sites to single out the effect of canopy structure. Only few studies have considered how the combination of forest and topography alter accumulation and melt processes

50 under forest relative to clearings. Ellis et al. (2011) presented measurements from a Canadian site, including short- and longwave irradiances and snow depth under the canopy and in clearings on different slopes and aspects, and showed that the presence of forest delayed snowmelt relative to open areas more strongly on south-exposed slopes than on north-exposed ones. In a modelling study, Strasser et al. (2011) found that forest cover diminished aspect-dependent differences in snow cover dynamics compared to openings, and further noted that forest effects differed between years with varying

55 meteorological conditions. Neither of these studies did, however, consider fine-scale canopy structural heterogeneity in detail, and no study that specifically addresses inter-annual consistency of fine-scale forest snow distribution patterns exists to our knowledge.

In recent years, the increased availability of LiDAR-derived snow depth distribution datasets has enabled a new approach to analysing forest snow cover dynamics, and multiple studies have attempted to establish relationships between snow, canopy,

60 and terrain descriptors based on such datasets (Zheng et al., 2019; Mazzotti et al., 2019a; Currier and Lundquist, 2018). Broxton et al. (2020) used maps of snow water equivalent and time series of snow depth transect measurements to analyse the combined impact of forest density and topographic location on snow water equivalent (SWE) dynamics in a semi-arid climate. Safa et al. (2021) applied machine learning to identify the factors that determine snow disappearance in different forest and topographic settings based on lidar-based snow depth maps covering four US sites with variable climate

65   characteristics. Recently, Koutantou et al. (2022) presented a time series of Uncrewed Aerial Vehicle (UAV) borne LiDAR datasets to compare the evolution of snow depth distribution patterns on opposed slopes in an Alpine valley. Despite all coming to interesting conclusions, these studies were limited to process inferences as snow distribution datasets only reflect the combined impact of forest snow processes.

Instead of relying on snow data alone, understanding process interactions can be advanced through sophisticated process-
70   based models. In absence of observational data, or for predictive purposes, models are commonly used as a best estimate of reality (Wood et al., 2011; Wrzesien et al., 2022). In forest snow research, the use of hyper-resolution models that resolve tree-scale processes is gaining popularity in applications that require the small-scale variability of these processes to be adequately represented (Harpold et al., 2020). To our knowledge, two models developed specifically for this purpose exist to date: SnowPALM - Snow Physics and LiDAR Mapping (Broxton et al., 2015) and FSM2 - Flexible Snow Model (Mazzotti
75   et al., 2020b, a), which evolved independent of each other but follow similar principles. Impact studies have used SnowPALM to analyse the effect of forest disturbance on snow water resources under varying meteorological conditions (Moeser et al., 2020), and to assess forest thinning strategies (Krogh et al., 2020). Hyper-resolution models also provide an approximation of processes that are not resolved in coarser resolution models and can thus inform the development of sub-grid parametrizations of these processes. As such, both SnowPALM (Broxton et al., 2021) and FSM2 (Mazzotti et al., 2021)
80   have been used to derive recommendations for modelling forest snow processes at coarser resolutions, and there is still great potential to further exploit these models as research tools.

In this study, we use hyper-resolution modelling to explore the spatio-temporal dynamics of individual forest snow processes and their effect on forest snow cover evolution in forested complex terrain under varying meteorological conditions. We apply FSM2 to a sub-alpine forested valley and across multiple winters to assess the interplay of canopy structure,
85   topography, and meteorology. Our work builds on Koutantou et al. (2022), who observed considerable differences in snow distribution dynamics between their sites located on south- and north-exposed forested slopes over the course of one snow season. The authors hypothesized that weaker correlations between snow depth and canopy cover at the south-exposed than at the north-exposed slope were due to differences in the shortwave irradiance regimes at the two locations but could not fully demonstrate this based on their data alone. The modelling approach used here, in contrast, will allow us to analyse
90   individual processes and their interactions over larger spatial and temporal extents than previously possible. Our goals are thus (1) to characterize spatial patterns of snow cover dynamics and the underlying processes in such a sub-alpine environment; (2) to detect connectivity between snow patterns and patterns of underlying processes; and (3) to assess their temporal consistency throughout the season and between different years. By contributing to the improved understanding of these complex dynamics, we hope to facilitate the development of approaches to treat sub-grid variability in coarser-
95   resolution models, and to help expand our capabilities to assess the impact of environmental change on ecohydrological processes.

2 Methods

2.1 Study area
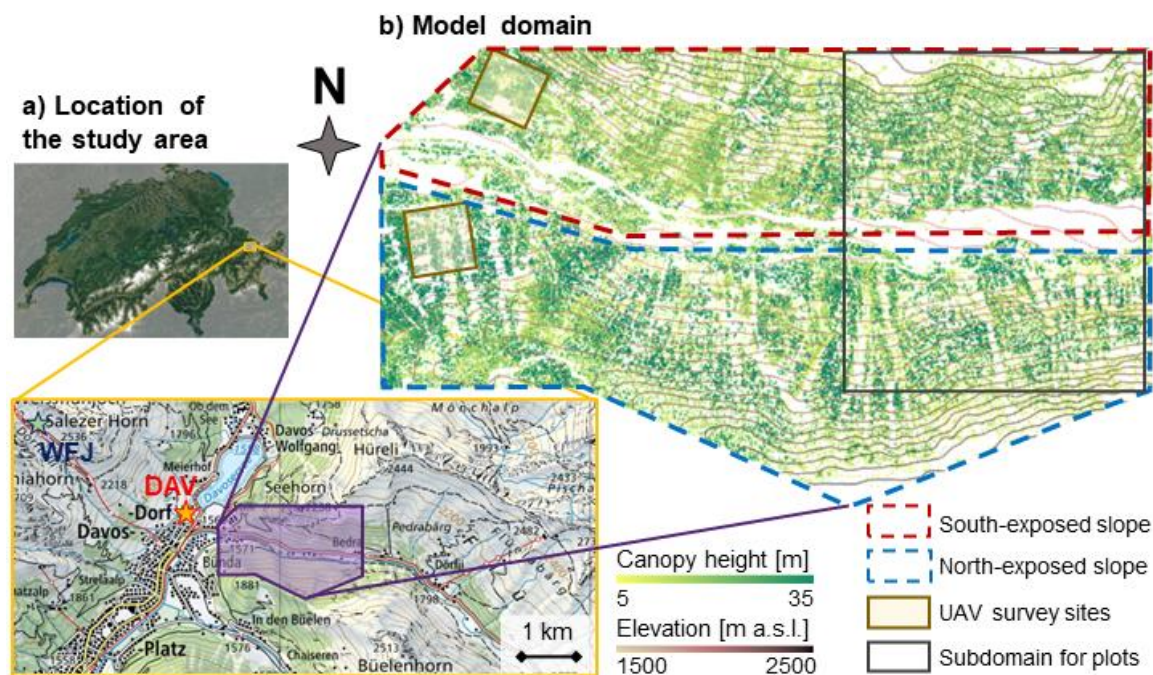
Figure 1: Overview of the study area: (a) Location of the model domain within Switzerland and on the topographic map of the Davos area, including locations of the automatic weather stations SLF and WFJ; (b) Canopy height model and contour lines (equidistance: 50m), including locations of the sites from Koutantou et al. (2022) and of the subdomain shown in Figures 5 and 7-9.

We focus our modelling in a domain situated in the Flüela valley near Davos (Figure 1) in the eastern Swiss Alps. The climate is inner-alpine with an average wintertime (DJF) air temperature of -4.2 °C and 450 mm yearly snowfall sum (Davos station, MeteoSwiss and SLF, norm period 1991-2020; www.meteoschweiz.ch). The model domain is contained in a 2.5 x 1.5 km area at the entry of the valley, which consists of two opposite (south- and a north-facing) slopes. Both slopes extend over 500 m elevation span from the valley bottom at 1570 m a.s.l. to the tree line around 2100 m. The forest is predominantly Norway spruce with some individual Larches, which is typical of this sub-alpine forest ecoregion. Trees range from new- to old growths with maximum heights of 35 m, and forest structure includes both dense stands and gaps of varied sizes. The domain thus spans a range of variability in canopy structure and topographic conditions over a rather small area, which is common in the sub-alpine environment. The site is at ~5 km distance to well-established and predominantly flat research sites that have hosted recent experimental forest snow process studies from the WSL Institute for Snow and Avalanche Research SLF, including Laret (Malle et al., 2019; Webster, 2016), Seehornwald (Webster et al., 2016), and Ischlag (Moeser et al., 2015). The sites from Koutantou et al. (2022) are fully contained in the perimeter of this study. The operational measurements from the automatic weather station (AWS) Davos (DAV) and from the measurement field at Weissfluhjoch (WFJ) are within 1 km and 3 km of the site, respectively.

2.2 Modelling framework

Snow cover simulations with the Flexible Snow Model FSM2 (Mazzotti et al., 2020b, a) are at the core of this study's methodology (see overview in Figure 2). FSM2 is the upgrade of the Factorial Snow Model, FSM (Essery, 2015), with forest

120 canopy included. We apply the version presented by Mazzotti et al. (2020a) specifically developed for hyper-resolution (meter-scale) simulations, which accounts for the influence of tree-scale canopy structure on individual forest snow processes by using process-specific canopy metrics. Notably, FSM2 can leverage detailed time series of point-scale transmissivity for direct shortwave radiation obtained with an external radiation transfer model. Past research has demonstrated that FSM2 is able to capture sub-canopy snow energetics by comparing model output to spatio-temporal multi-

125 sensor datasets, for incoming irradiances, air space and snow surface temperature, and wind speed (Mazzotti et al., 2020a). Consequently, FSM2 has been shown to accurately replicate small-scale forest snow cover dynamics and the respective microclimatic states (Mazzotti et al., 2020b, a). For this study, we run FSM2 at 2 m grid spacing (i.e., 850'000 points) for 6 winters (i.e., water years (WY) 2016-2021). Our model application follows Mazzotti et al. (2021), who used equivalent hyper-resolution simulations to explore model upscaling behavior.
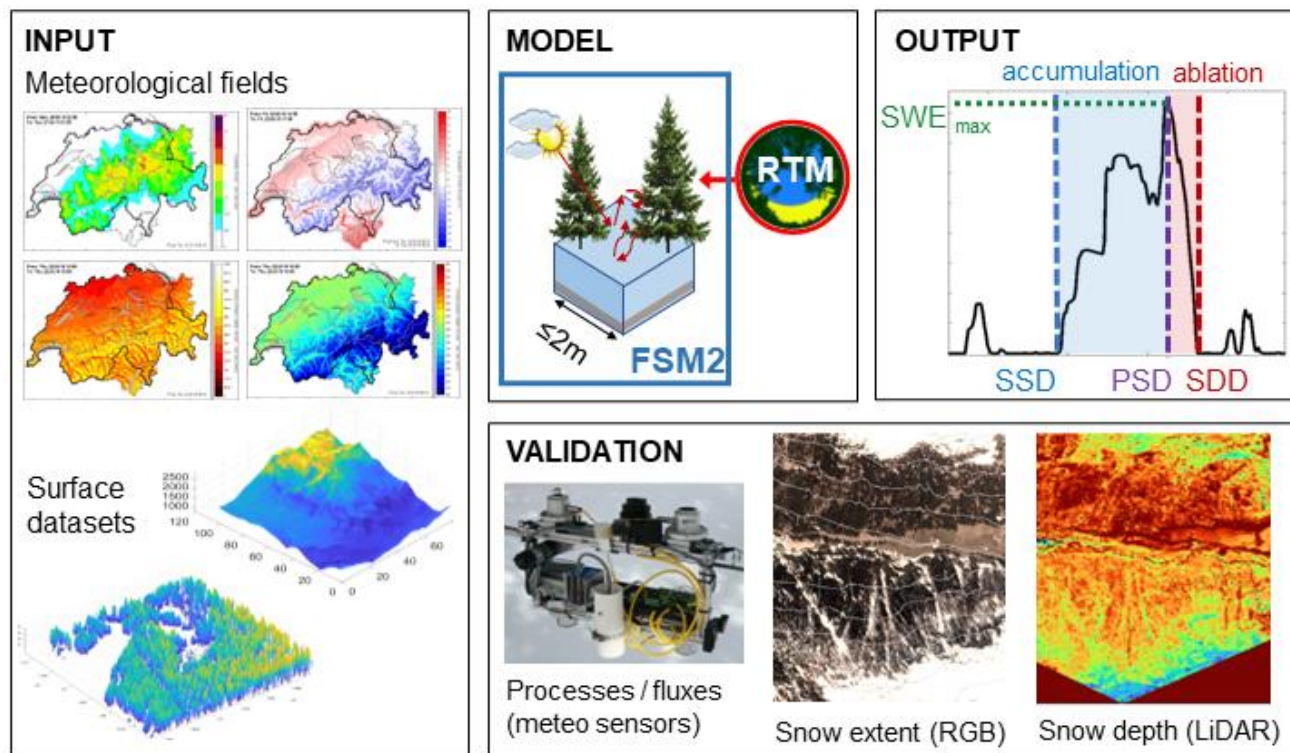
130

Figure 2: Conceptual sketch of the study methodology. Input meteorological and surface datasets (from the OSHD and the 2017 LiDAR mission, Section 2.2), FSM2 including external radiation transfer model, evaluation approaches (presented in Mazzotti et al. 2020a and Section 2.3) and resulting snow cover dynamics descriptors (definitions see Section 2.4).

LiDAR datasets acquired through airborne laser scanning (ALS) in 2017 in the context of the first European mission of the

135 Airborne Snow Observatory (Painter et al., 2016; Mazzotti et al., 2019a) provided the basis for computing all canopy metrics required by FSM2, including the shortwave transmissivity time series. A canopy height model was created following the LAStools-based algorithm from Khosravipour et al. (2014), enabling calculation of local and stand-scale canopy cover fraction, mean canopy height, and leaf area index at all modelled locations. Details on the individual metrics are given in Mazzotti et al. (2021, 2020b). Shortwave transmissivity time series at each location were obtained with the workflow from

140 Webster et al. (2020), which calculates time-varying transmissivity through an overlay of a hemispherical image and solar position at any given point in time, as presented by Jonas et al. (2020). In the model from Webster et al. (2020), LiDAR-based synthetic hemispherical images based on a methodology originally proposed by Moeser et al. (2014) are used for this purpose. The radiation model was calibrated using real hemispherical images at our sites and using the same LiDAR data (Koutantou et al., 2022), allowing direct application in this study. Additional surface datasets (e.g., elevation) were available

145 through SLF's Operational Snow-Hydrological Service's (OSHD) modelling framework. These data were provided at 25 m resolution and interpolated to the model resolution (2 m).

Meteorological forcing was also available from the OSHD. As described by Griessinger et al. (2019), gridded data of all necessary meteorological input variables (incoming short- and longwave radiation, air temperature and relative humidity, wind speed, rain- and snowfall rates, and atmospheric pressure) are provided by MeteoSwiss (COSMO-1 product) at hourly

150 interval and 1-km resolution over all of Switzerland and further downscaled to model resolution. Additional corrections (for biases or terrain effects) are applied to some of the variables, e.g., wind speed (Winstral et al., 2017) and shortwave radiation (Jonas et al., 2020). We refer to Griessinger et al. (2019) for details. For this study, input fields were initially downscaled to 25 m and subsequently linearly interpolated to 2 m resolution.

2.3 Verification of model use case

155 The validation of individual modelled fluxes within FSM2 as presented by Mazzotti et al. (2020a) was done in the vicinity of our study area, with the same type of input data, and for the same type of canopy data. For this reason, another model validation is beyond the scope of this study; nevertheless, an assessment of our simulations against available snow distribution datasets was performed to ensure plausibility of the model application for our use case. We use four independent data sources: (1) Snow depth data acquired by automatic weather stations (AWS) in Davos and Weissfluhjoch to assess the

160 simulations at open sites; (2) High- and medium-resolution satellite RGB imagery available through Planet Explorer (www.planet.com) at approx. weekly intervals for the last five modelled WY's, including Landsat 8, Sentinel-2 and PlanetScope, to evaluate modelled snow cover extent during periods of partial snow cover; (3) Snow depth distribution maps over the full domain from two of the 2017 ASO LiDAR acquisitions (see Section 2.2) at 3 m spatial resolution, parts of which were used by Mazzotti et al. (2019a); and (4) Time series of snow depth maps over two 150 x 150 m domains (see

165 Figure 1) on the two opposed slopes obtained with a UAV-borne LiDAR in 2020, presented by Koutantou et al. (2022).
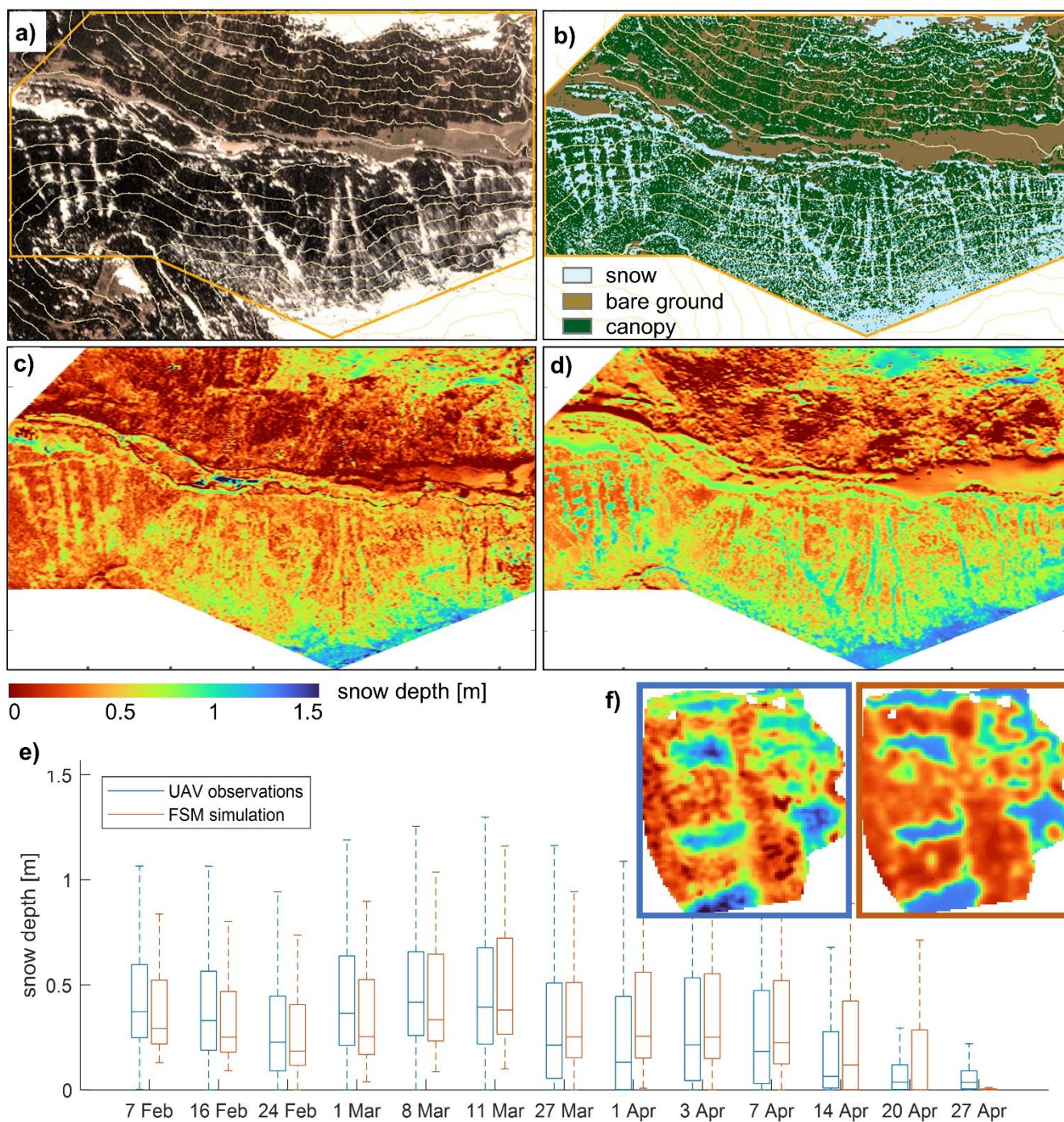
Figure 3: Examples of plausibility checks performed to verify the model use case, including comparisons of 1) satellite RGB imagery acquired by Planetscope on 28. April 2018 (a) and snow cover extent simulated by FSM2 on the same day (b); 2) snow depth distribution derived from ALS data (c) and simulated by FSM2 (d); and 3) snow depth statistics of UAV-LiDAR derived snow maps at the north-exposed site and resulting from FSM2 (e) and observed and modelled spatial distribution of the 8 March 2020 campaign (f).

170

Figure 3 presents examples of visual comparisons of model simulations to satellite (Figure 3a-b), ALS (Figure 3c-d) and UAV-LiDAR data (Figure 3e-f). These assessments reveal the model captures the general characteristics of snow depth and melt out patterns well. The strong temporal lag in melt out between the south- and the north-facing slope is clearly visible in

175 the satellite imagery and likewise reproduced by the FSM2 simulations. Snow distribution features such as preferential melt along south-exposed forest edges and higher snow amounts in canopy gaps compared to nearby under-canopy locations in the north-exposed slope are also clearly present in both the LiDAR datasets and the simulations. Overall, the verification confirms that FSM2 simulations are suitable for this use case.

2.4 Analysis approach

180 Our analysis uses several descriptors of the snow season and of the surface energy exchange processes derived from the FSM2 simulation results. These metrics are computed at each modelled location (i.e. 2 m grid cell) for all winters as follows.

1. *Peak SWE:* The maximum value of snow water equivalent attained over the course of a snow season / WY.
2. *Day of peak SWE (PSD):* The day on which peak SWE occurred. In case of multiple occurrences of peak SWE over the season, the median was selected.
185 3. *Accumulation period:* Period between the last occurrence of SWE < 10 mm prior to peak SWE and the day of peak SWE.
4. *Start of snow cover period (SSD):* The first day of the accumulation period.
5. *Ablation period:* Period between the day of peak SWE and the first occurrence of SWE < 10 mm following peak SWE.
190 6. *Snow disappearance day (SDD):* The last day of the ablation period.
7. *Snow cover duration:* The number of days between the start of snow cover and snow disappearance.
8. *Ablation rate:* The quotient between peak SWE and the length of the ablation period.
9. *Cumulative melt:* Amount of SWE depleted over the course of a specific time interval.
10. *Average surface energy fluxes:* Incoming and net short- and longwave radiation as well as turbulent (sensible and
195   latent) heat fluxes into the snowpack, averaged over a specific time interval, where positive fluxes indicate transport towards the snow surface.

Note that the temporal integration varies for different metrics, with some applying to the point-specific snow cover durations and some integrating over fixed time intervals. The choice of temporal integration interval is motivated by the purpose of the respective analysis and details are given where they appear. Moreover, it should be noted that the definition of contiguous

200 accumulation and ablation periods until / from peak SWE as applied here, implies that melt events can occur during the accumulation and snowfall events during the ablation periods, respectively.

To assess relationships of any snow or process descriptor to canopy structure, we quantify the fine-scale canopy structure at a point in terms of local canopy cover fraction, one of the canopy metrics provided as input to FSM2 ('fveg', see Mazzotti et al. (2020b)). This variable describes the fraction of the vertically projected canopy cover within a 5 m radius around each

205   modelled location, taking values between 0 and 1. We used local canopy cover fraction because it was shown to be strongly
correlated to small-scale snow depth distribution at flat sites (Mazzotti et al., 2020b) and in steep terrain (Koutantou et al.,
2022).

3 Results

In the following sections, we first provide a general overview of snow cover dynamics across the site for all simulated years
210   to provide context (Section 3.1), then consider the spatial distribution of our snow descriptors in more detail (Section 3.2).
To help interpret spatial patterns, we analyse the combined impact of the physiographic factors, topography and canopy
structure, first on the temporal evolution (Section 3.3) and then on the spatial distribution (Section 3.4) of snow cover
dynamics and the underlying processes. Finally, we explore the impact of meteorological conditions on the temporal
consistency of said spatial patterns between water years (Section 3.5).

215   ### 3.1 Overview of simulated snow cover dynamics

Figure 4 summarizes the statistics of the different snow season descriptors for all simulated years, aiming to provide an
overview of their within-year variability (attributable to variations in canopy structure and topography), and of their
between-year variability (attributable to variations in driving meteorology). A summary of meteorological conditions during
the simulation period is provided in the Supplementary Material (S1). The start of continuous snow cover strongly varies
220   both across the model domain and between the years (Figure 4a). The medians within the model domain vary by 2 months,
ranging from 5 November (WY 2019) to 5 January (WY 2017). Noteworthily, the spread of the start of snow cover varies
strongly between the simulated WYs as well. While in three years snow cover onset happens basically simultaneously across
the entire domain (WYs 2017, 2018, 2019), partial melt-out during snow accumulation cause heterogeneous snow cover
onset dates across the domain in the other years, with interquartile ranges of full snow cover onset of over a month.
225   The timing of peak SWE (Figure 4b) is, on average, much more consistent over the years, with median peak SWE ranging
from 11 March (WY 2020) to 1 April (WY 2018). However, the spread across the model domain in each year can be large
(interquartile range of approx. 2 months in WYs 2019 and 2021), which means that there can be a considerable temporal
offset in the start of the ablation period across the site. Notably, this leads to some locations reaching peak SWE only when
others have melted out already (overlap of boxes for day of peak SWE and snow disappearance day of the same year). The
230   rather large spread in snow disappearance day within each year (Figure 4c), with interquartile ranges between 2 and 6 weeks,
is the result of spatial variability in both accumulation and ablation rates and is thus not surprising. Between-year variability
in melt-out timing is much larger than for timing of peak SWE, with medians between 10 April (WY 2016) and 26 May
(WY 2019). Further, also peak SWE itself varies (Figure 4e), with median peak SWE across the model domain between 135
mm (WY 2016) and 314 mm (WY 2019), mostly reflecting years with higher and lower snowfall, respectively. Notably,
235   interquartile ranges are not systematically higher or lower for higher or lower median peak SWEs occurrences.
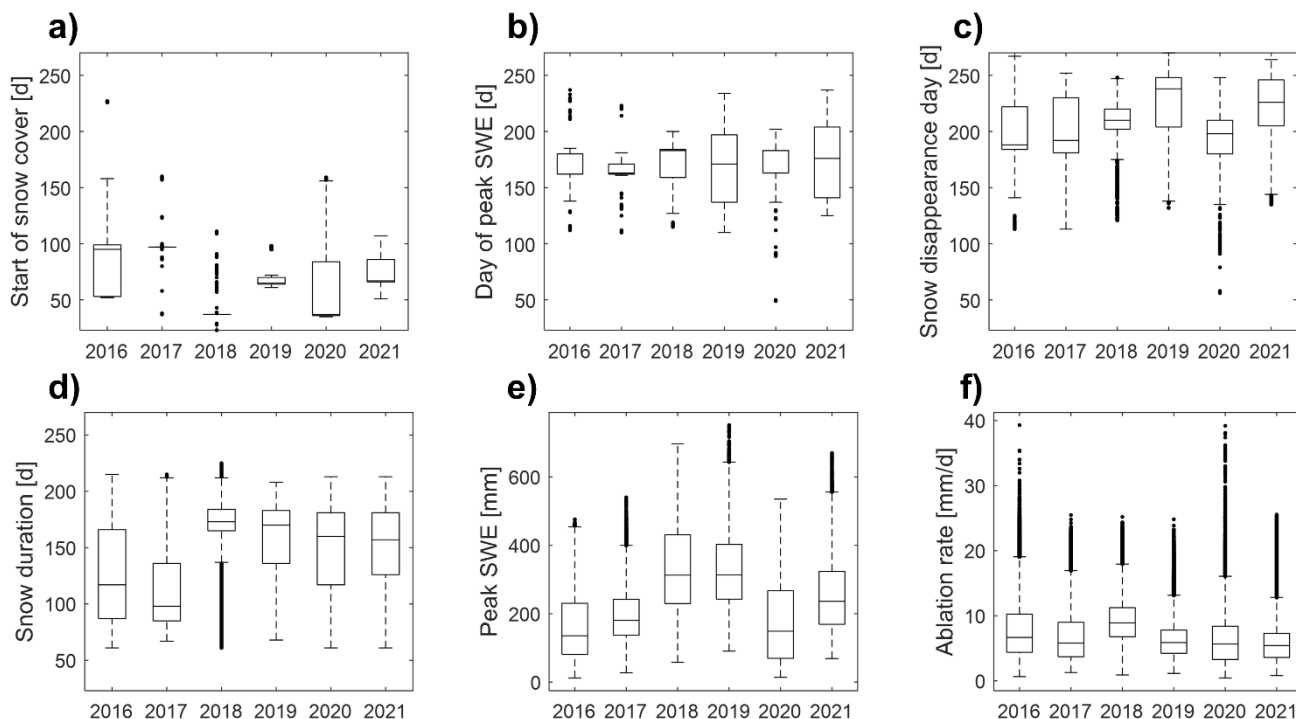
Figure 4: Summary statistics of snow season descriptors across the full model domain and for all simulated water years (WY), including (a) the start of snow cover period, (b) day of peak SWE, (c) snow disappearance day, (d) duration of full snow cover, (e) peak SWE, and (f) ablation rate. Descriptors denoting specific points in time (a-c) are indicated in terms of day since October 1st.

240 The combination of the variable start of snow cover and snow disappearance days implies highly variable snow cover durations (Figure 4d). Median full snow cover duration across the model domain varies between 96 (WY 2017) and 173 (2018) days, and interquartile range varies between 19 (WY 2018) and 65 (WY 2020) days. Snow cover duration can also be interpreted as the combination of amount of SWE available for melt and efficiency of melt processes. Notably, ablation rates (Figure 4f) are more uniform across the WYs (median 5.5-9 mm/day) but still rather variable across the model domain

245 (interquartile ranges of 3.6-5.9 mm/d).

It should be highlighted that there does not appear to be any clear link between any of the snow cover descriptors; for instance, higher peak SWE does not seem to imply longer snow duration, and later snow disappearance is not linked to higher melt rates. Essentially, this is a consequence of accumulation and ablation processes being affected by different meteorological drivers.

250 **3.2 Spatial patterns of snow cover dynamics**

Large spread in the boxplots in many of the subpanels of Figure 4 indicates that most snow season descriptors exhibit strong spatial variability across the model domain during most years. In Figure 5, we present spatial maps of the same snow season descriptors for WY2019 to analyse the full spatial patterns behind this variability. To better demonstrate the spatial details,

we zoom in to a sub-domain (Figure 1) that covers the entire range of canopy structures, elevation ranges, slopes, and aspects, yet representing the physiographic character of the entire domain well. Equivalent plots over the full model domain are included in the Supplementary Material (S2) for interested readers.
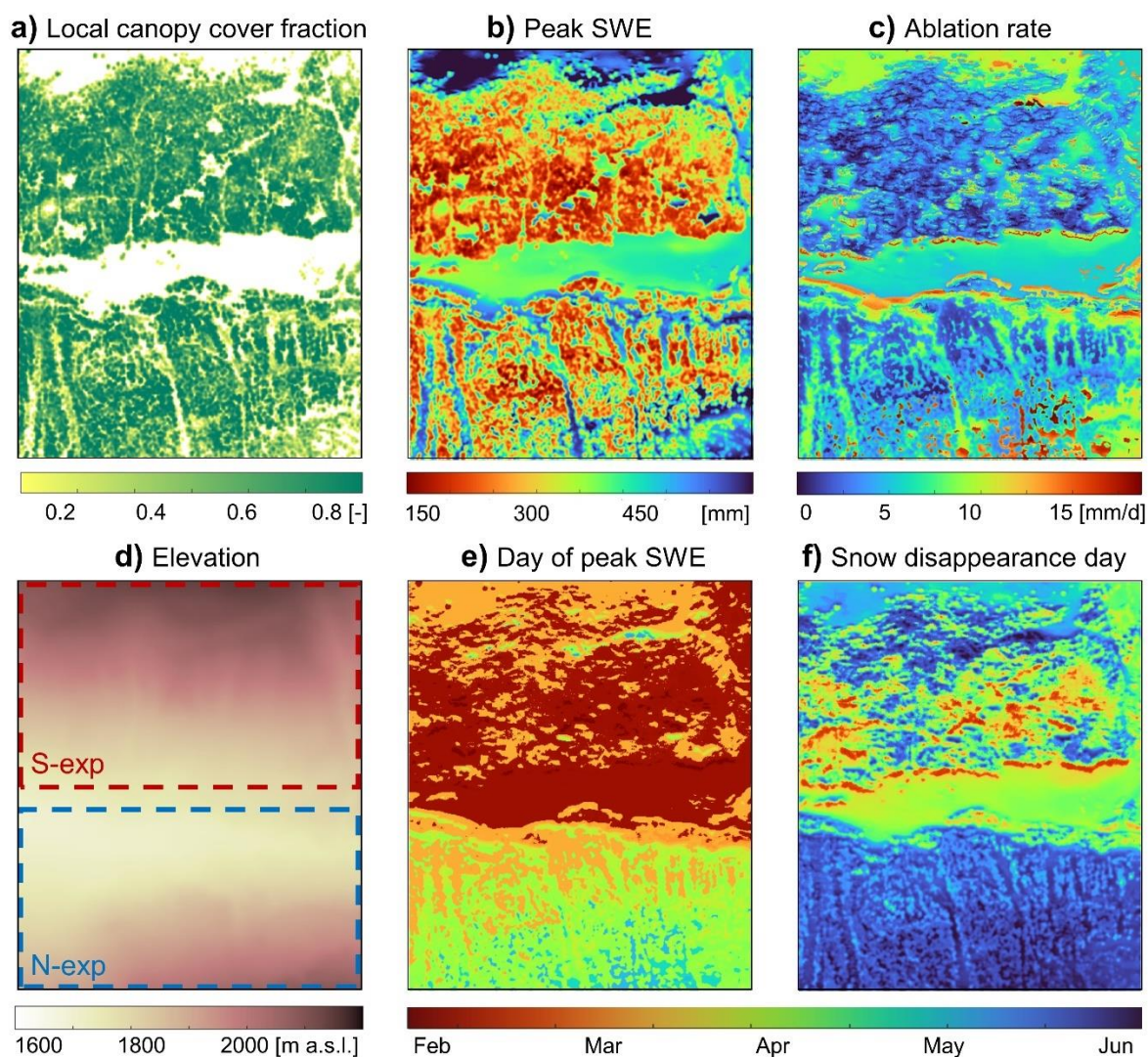
Figure 5: Canopy cover (a) and topographic (d) maps, as well as snow season descriptors including peak SWE (b), ablation rate (c), day of peak SWE (e) and snow disappearance day (f), for a sub-section of the model domain and WY 2019.

Figure 5 illustrates how peak SWE, ablation rates, day of peak SWE, and melt-out date vary across the landscape as a function of canopy and within the complex topography. The link between peak SWE and canopy structure (Figure 5a vs 5b) is obvious and reflects the impact of snow interception by the canopy on accumulation, which scales with local canopy cover. This dependency is well visible when comparing peak SWE at under-canopy vs. open / gap locations. Yet, a closer look at the gaps and forest edge areas (especially in the upper, south-exposed part of the domain) reveals a rather large

265   spread in peak SWE for these locations with low to no local canopy cover, even within this relatively small subdomain of 1.5 km^2. For this specific example, the spread in peak SWE amounts to approx. 200 mm. Consequently, canopy structure is clearly not the only factor controlling peak SWE distribution, despite the strong correlation between peak SWE and local canopy cover fraction with Pearson's correlation coefficient (R) ranging from -0.89 (2018) to -0.76 (2017).

When interpreting spatial patterns of peak SWE, it is important to consider that the timing of peak SWE also varies across

270   the domain (i.e., ablation starts in some areas while others are still accumulating snow; Figure 5e). Generally, the onset of the ablation period occurs earlier on the south-exposed slope. The earliest onsets occur along the canopy edge at lower elevations, but there is no evident simple relationship with canopy structure. The combination of strong variability in peak SWE and heterogeneous peak SWE timing means that spatial patterns of ablation rates (Figure 5c) and snow disappearance date (Figure 5f) are complex, with non-trivial dependencies with either canopy structure or topography (Figure 5d).

275   Notably, snow disappearance day is more variable on the south-exposed slope than in the north-exposed slope, where snow disappearance is restricted to a shorter time span. Complex melt-out patterns on the south-exposed slope hint at considerable spatial heterogeneity in melt processes which override accumulation patterns, so that the spatial structure of snow disappearance is considerably different from that of peak SWE (Figure 5b vs 5f, upper part). In contrast, this is not the case on the north-exposed slope: Here, under-canopy areas melt out earlier than canopy gaps, which means that melt-out patterns

280   generally have a similar spatial distribution as accumulation patterns (Figure 5b vs 5f, lower part). These similarities suggest that on the north-exposed slope spatial variations in melt rates are not strong enough to supersede spatial variations in accumulation. We will look at the physical processes that drive these patterns in more detail in the following sections.

Ablation rates (Figure 5c) exhibit spatial patterns that do not correspond to any other snow season descriptor. Notable features are the maxima along the south-facing canopy edge on the south-exposed slope, and in the canopy gaps on the

285   higher-elevation areas of the north-exposed slope. This is where snow generally either starts to melt first or last (compare to Figure 5e). Furthermore, large canopy gaps on both slopes generally feature higher melt rates than adjacent under-canopy areas. Note that assessing the dependencies of melt rate on canopy structure and topography is confounded by the necessity to calculate melt rates over the local melt period (see definition in Section 2.4), which itself varies across the domain due to variable timings of peak SWE and snow disappearance.

290 **3.3 Impact of canopy structure and topography on the temporal evolution of the snow cover and underlying processes**

The analysis in Section 3.2 clearly suggests that the interaction between canopy structure and topography plays a relevant role in shaping spatial snow cover dynamics. To understand these patterns and the processes that lead to them, it is instructive to consider time series of snow cover evolution at some representative locations. We selected seven locations that cover the existent range of canopy structures and topographic settings to showcase potential outcomes of process interactions

295   in a systematic way. We include points located at the north- and south-facing edges of canopy gaps for both north- and south-exposed slopes, as well as three points located under canopy (two on the south- and one on the north-exposed slope, where the two points on the south-exposed slope differ in their proximity to a sun-exposed canopy edge). The locations of

these points are marked in the Supplementary Material (S3). Figure 6a shows SWE at these seven locations for WY 2019. Note that we will look at data from other years and the influence of weather on inter-annual differences in Section 3.5.

300 At the beginning of the accumulation period, the three points that are located under canopy accumulate less snow than all points located in gaps. This reflects the fact that, if no major precipitation gradients exist across the site and if melt or the impact of wind redistribution is negligible, interception of snow is the only process that introduces spatial variability during this phase. Early season, all under-canopy points and all points in canopy gaps thus follow distinct pathways, respectively, confirming that canopy structure exerts the primary control on snow accumulation. However, as the season progresses,

305 further pathways fork off. In this example, early onset of ablation at two points on the south-exposed slope results in further spatial segregation. The first point (dark red), which reaches peak SWE by mid-February, is located under canopy close to a south-facing canopy edge. The second point (light green), which reaches peak SWE in mid-March, is located at the south-facing edge of a forest gap. These findings showcase that the same canopy structure configuration can host different snow evolution pathways in different topographic settings. This creates more variability in snow cover evolution pathways on the

310 south-exposed slope (here, points at south- and north-facing canopy edges diverge), and limited variability on the north-exposed slope (here, points at south- and north-facing canopy edges do not diverge).
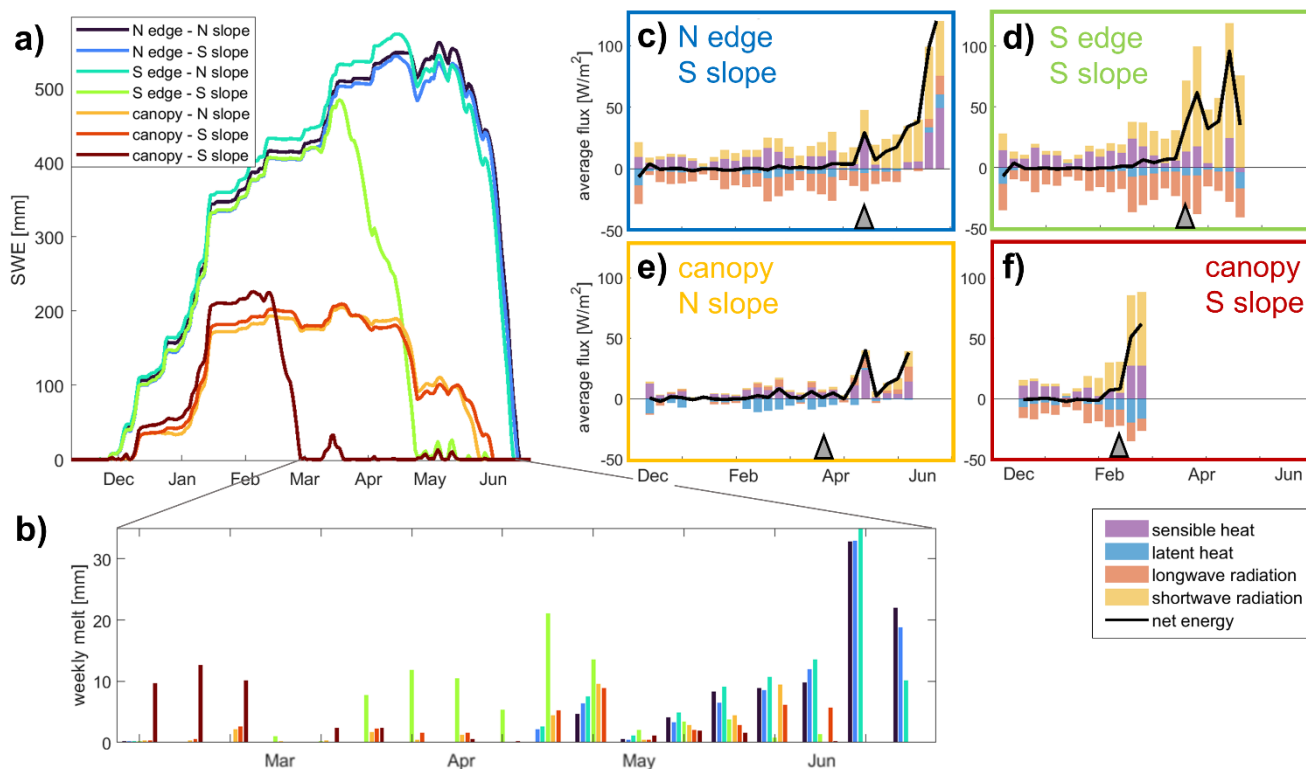
Figure 6: Interactions between canopy structure and topography illustrated at seven example points (locations see S3). Time series of SWE (a), weekly melt during the ablation period (b) and surface energy balance partitioning at four of the points (c-f). In c-f,
315 **bars show weekly average fluxes, while the black line depicts their sum, grey triangles mark the day of peak SWE, and only periods with snow on the ground are shown.**

While accumulation patterns are mainly dictated by canopy structure, topography comes into play when ablation processes start. Melt requires a positive net energy input to the snowpack, which is the result of multiple superimposed fluxes. To elucidate the underlying processes, Figure 6c-f show surface energy balance partitioning over time at four of the seven

320   points, which cover the four major snow cover evolution pathways seen in Figure 6a. These plots show that at all points prior to the onset of the ablation period, net shortwave radiation and sensible heat generally provide positive contributions, while latent heat provides a negative contribution. Longwave radiation acts as a compensating flux. It is strongly negative at locations in canopy gaps (large sky-view, i.e., little longwave enhancement, Figure 6c+d) as well as under-canopy locations that receive positive shortwave radiation and sensible heat contributions, but positive where other positive fluxes only

325   constitute negligible contributions (i.e., under-canopy, shaded locations, Figure 6e). At both points where ablation starts early, regardless of canopy structure, its onset is due to an increase in net shortwave radiation that can no longer be compensated by a negative longwave radiation flux. Exposure to shortwave irradiance early in the snow cover period is thus a mechanism by which topography can affect snow cover evolution pathways in addition to canopy structure, either by way of terrain shading or due to inclined terrain (towards or away from sun). At points where direct insolation is unavailable

330   early in the snow cover period and ablation starts later, the driving mechanisms are different. At under-canopy points, positive longwave radiation contributions and sensible heat drive melt; at gap locations, shortwave radiation and sensible heat constitute the strongest positive fluxes.

Generally, shortwave radiation driven melt leads to larger net energy turnover and therefore high melt rates even early in the season (Figure 6b). This can create situations where snow in canopy gaps can actually melt out earlier than snow under

335   canopy, despite peak SWE being higher (Figure 6a, light green vs light red). Early-season insolation is hence the driver by which spatial heterogeneity in melt processes can override accumulation patterns on the south-exposed slopes (c.f. Section 3.2). Not surprisingly though, the highest melt rates are in the late season in gaps when all fluxes are positive. Yet these high melt rates do not impact melt-out patterns, because by this time gaps on the north-exposed slopes are the only areas with snow left.

340   **3.4 Impact of canopy structure and topography on the spatial distribution of leading processes**

The snow cover evolution pathways and corresponding energy balance partitioning pathways shown in Section 3.3 illustrate the interaction between canopy structure and topography. Considering how these pathways are distributed in space puts the snow cover descriptor maps from Figure 5 in context. An important insight from Section 3.3 is that exposure to early-season shortwave radiation majorly affects snow cover dynamics, which leads to contrasts between opposing slopes that are or are

345   not affected by terrain shading. Figure 7 shows maps of canopy structure, average shortwave irradiance, all-wave irradiance, and cumulative snowmelt between mid-January and end of February for WY 2019 across the two opposing slopes. This period was chosen because it falls between the start of the snow cover period and median day of peak SWE, which makes it suitable for analysing the occurrence and distribution of early-season melt.

a) Canopy cover fraction **b)** Shortwave irradiance **c)** All-wave irradiance **d)** Snow melt
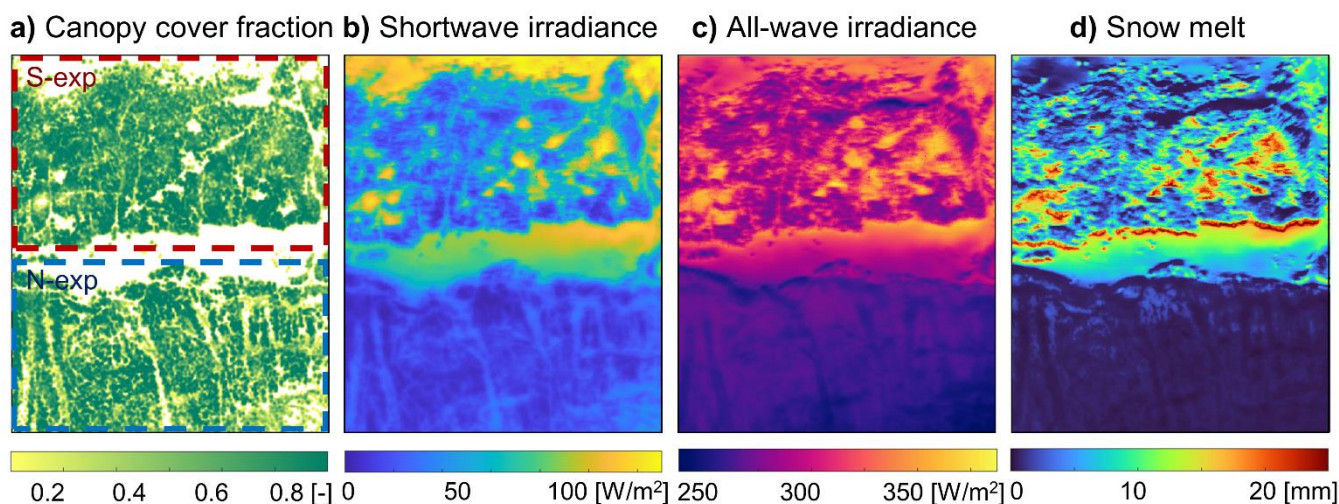
350 **Figure 7: Canopy structure and aspect in the sub-domain (a), average incoming shortwave (b) average all-wave irradiance (c), and cumulative snowmelt (d) between mid-January and end of February for WY 2019.**

In early winter, shortwave irradiance controls all-wave irradiance patterns (Figure 7b vs. 7c; see also Figure S2.3 in Supplementary Material, S2), and snowmelt largely matches these patterns (Figure 7d), confirming that early-season shortwave irradiance is a prerequisite for early-season melt. Due to topographic shading, only the south-exposed slope

355 receives direct shortwave irradiance at this time of the year. Consequently, topography exerts a primary control on early-season melt. On top of that, canopy shading affects the distribution of shortwave irradiance, but during times with low solar elevation angles the dependency between canopy structure and direct shortwave radiation is complex. In fact, early in the season the correlation between shortwave irradiance and local canopy cover is rather low (R = -0.52). This, in turn, entails local canopy cover and snowmelt to be uncorrelated as well (R = 0.05). These low correlations imply that early-season melt

360 may potentially counteract and even disrupt the association of peak SWE patterns and local canopy cover identified in Section 3.2 (see Figure 5).

Shortwave irradiance is, however, not the only flux determining melt patterns. Figure 7 reveals that some areas above the tree line on the south-exposed slope do not experience early-season melt, despite the high shortwave radiation input, therefore net energy input must be reduced by other negative fluxes. Additionally, the energy balance partitioning plots in

365 Figure 6 indicate other positive contributions to melt energy. To visualize the spatial structure of these contributions, Figure 8 shows each individual surface energy balance component for periods early (Figure 8a) and late (Figure 8b) in the season (WY 2019), as well as the corresponding net surface energy flux (Figure 8c). The spatial distribution of individual energy fluxes and their evolution in time generally conform with findings from Figure 6, with sensible heat as the only other positive contribution early in the season and longwave transitioning into a positive flux especially at under-canopy locations

370 and later in the season. Overall, Figure 8 demonstrates how spatial patterns of individual fluxes translate to patterns of net surface energy, which largely match shortwave radiation patterns in both periods. Figure 8d displays correlation coefficients

between net surface energy and individual energy balance components as they evolve over the season. The strongest positive correlations to shortwave radiation are confirmed, while correlations to longwave radiation are consistently and increasingly negative. No systematic link between net energy and turbulent fluxes is evident.
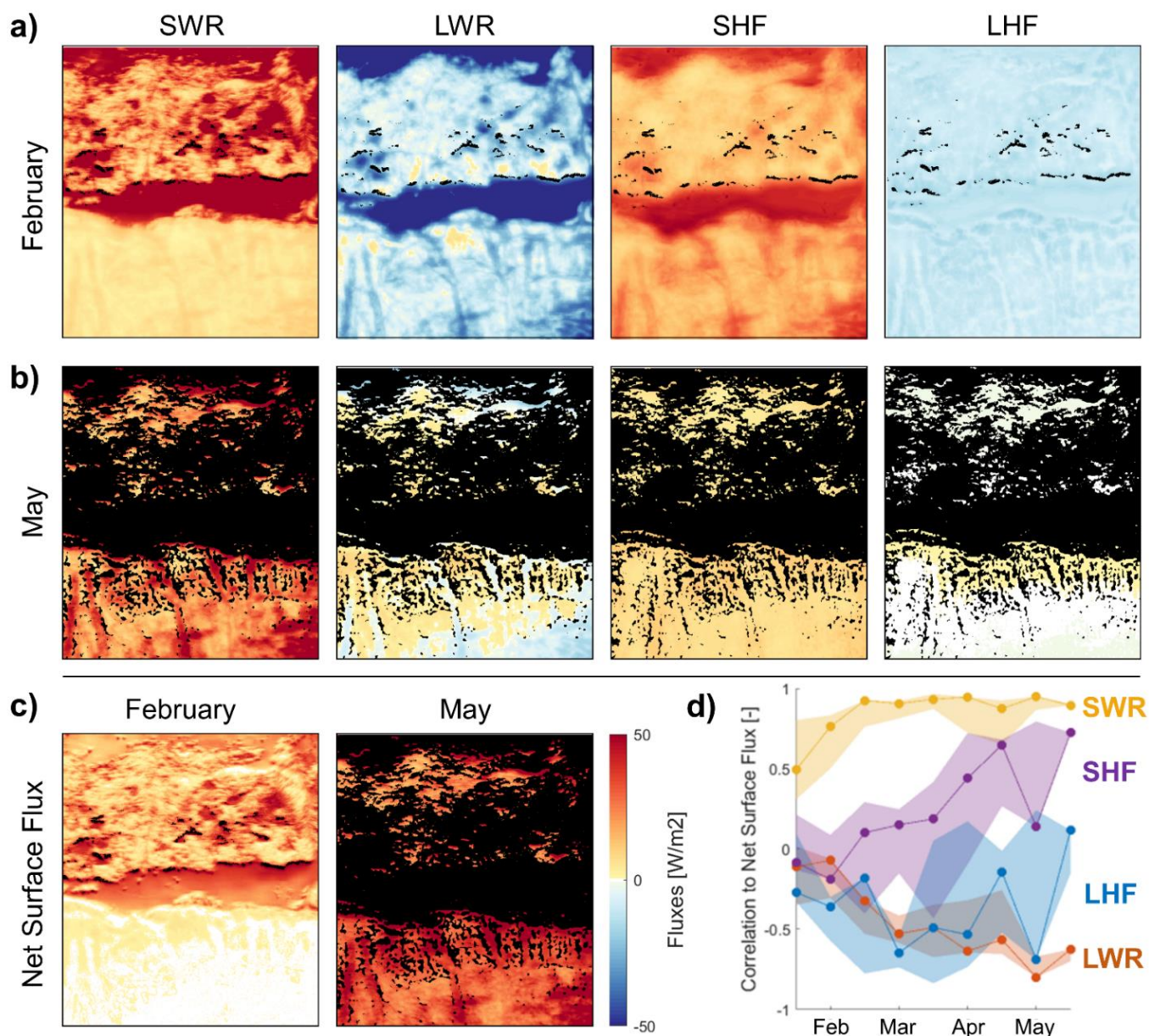
Figure 8: Energy flux partitioning into the four surface energy balance components for two weeks in February (a) and May (b) 2019, respectively, as well as net energy flux at the snow surface (c), areas that have melted out by the time shown are marked black; Correlations (Pearson's R) between individual energy fluxes and net surface energy over the season (d), with lines showing WY 2019 and shaded areas the range of all modelled WYs.

375

380   **3.5 Impact of meteorological conditions on the temporal consistency of spatial patterns**
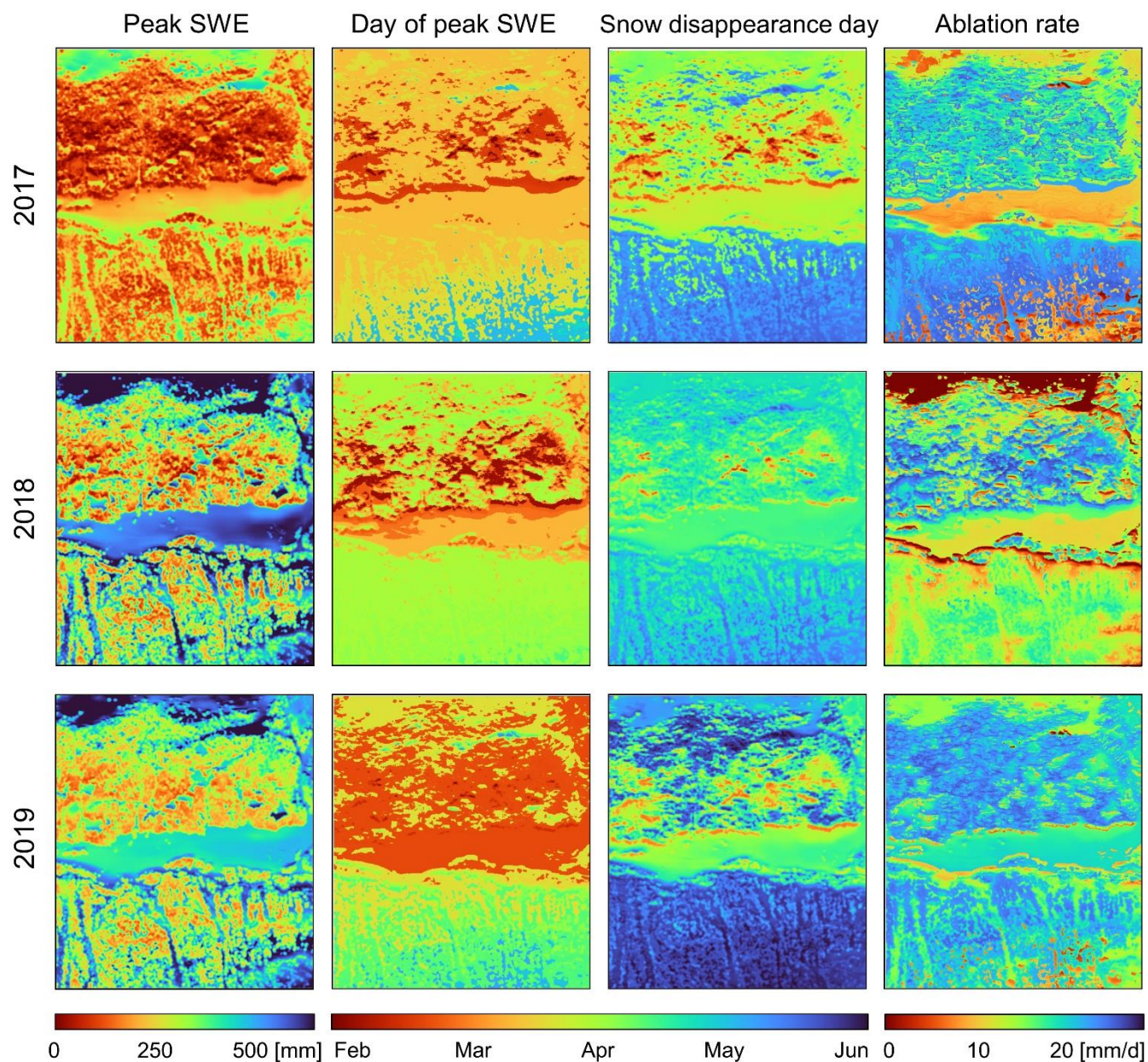
Figure 9: Spatial patterns of snow season descriptors for the sub-domain, including peak SWE (1st column), day of peak SWE (2nd col.), snow disappearance day (3rd col.) and ablation rate (4th col.) during three different WYs, namely 2017 (1st row), 2018 (2nd row) and 2019 (3rd row).

385   Meteorological conditions and their variability between years alter the relative magnitude and timing of different processes. By doing so, they can potentially impact the consistency of snow cover dynamics and resulting spatial patterns. Figure 9

shows the spatial distribution of the same snow cover descriptors shown in Figure 5, but now including three different WYs. For all snow season descriptors, we find both temporally consistent and inconsistent features. The link between canopy structure and peak SWE is evident in all years, despite stronger imprints of early-season melt patterns in some years (e.g.

390 2018 vs. 2019). In fact, the autocorrelation between peak SWE patterns of different years is high (R: 0.94-0.98). In contrast, ablation rate patterns are generally uncorrelated (R: 0.07-0.79). Ablation rate maxima are found at different locations of the domain in different years. For example, maximum melt rates in WY 2018 were above the tree line on the south-exposed slopes but were in canopy gaps on the north-exposed slope in both WYs 2017 and 2019. Below-canopy areas have comparatively low melt rates in all years, but differences between slopes are more pronounced in WY 2018 than in 2017 and

395 2019. These consistencies and inconsistencies are likely affected by differences in the timing of the ablation period.

In terms of the timing of peak SWE and snow disappearance, the temporal sequence in which different locations melt out is mostly consistent between years: South-exposed canopy edges and under-canopy locations generally become snow-free first, and snow lasts longest in shaded canopy gaps (i.e. those on north-exposed slopes). However, the timing of and days between both peak SWE and snow disappearance across the domain vary. For example, distribution of peak SWE day in 2019 is, in

400 the first order, bimodal, with a clear separation between the south- and north-exposed slopes; also in 2017, the distribution of peak SWE day is approximately bimodal, but in this case with a separation of only the sunny forest edges on the south facing slope, reflecting a considerably smaller number of pixels that exhibit sufficient early-season melt to prepone peak SWE day relative to all other pixels.

Analogous to our approach in Section 3.3, we consider time series at point locations to unravel the process-level mechanisms

405 that cause potential inconsistencies in snow cover descriptor patterns between years (Figure 10). To better highlight these inter-annual variations, we focus on a set of points located in semi-open conditions on the south-exposed slope, i.e., where they can potentially receive early-season direct shortwave radiation (locations see Supplementary Material S3). These include a point in a large gap, close to the south-facing canopy edge (yellow); a point in a smaller gap (dark red); and two points under relatively sparse canopy in rather sunny (dark blue) and a shady (cyan) locations, respectively. Due to the

410 limited range in local canopy cover at these points, the differences in accumulation caused by interception are less pronounced than for the examples shown in section 3.3 (c.f. Figure 10 vs. Figure 6). Yet, these points experience different drivers of ablation and therefore react differently to variations in meteorological conditions between the years.

Firstly, we note that accumulation patterns (i.e. peak SWE) vary between years based on the timing of the first melt events relative to the timing of peak SWE, particularly whether or not considerable melt events occur during the accumulation

415 period (Figure 10a). In 2019, when all major snowfall events occur prior to the first melt episode, gaps feature the highest peak SWE, corresponding to low interception losses (yellow and red). In 2017 in contrast, overall accumulation is low, and substantial melt precedes the last major accumulation event, which is sufficient to cause melt-out at some of the most sun-exposed locations; peak SWE at the sunny canopy gap point (yellow) is now thus the lowest of the four points considered. It should be noted that for all WY's considered here, onset of full snow cover happened roughly simultaneously across the

420 entire model domain; early melt events leading to partial melt-out prior of the onset of full snow cover (not shown, but observed e.g. in WY 2016) would obviously further complicate peak SWE patterns.
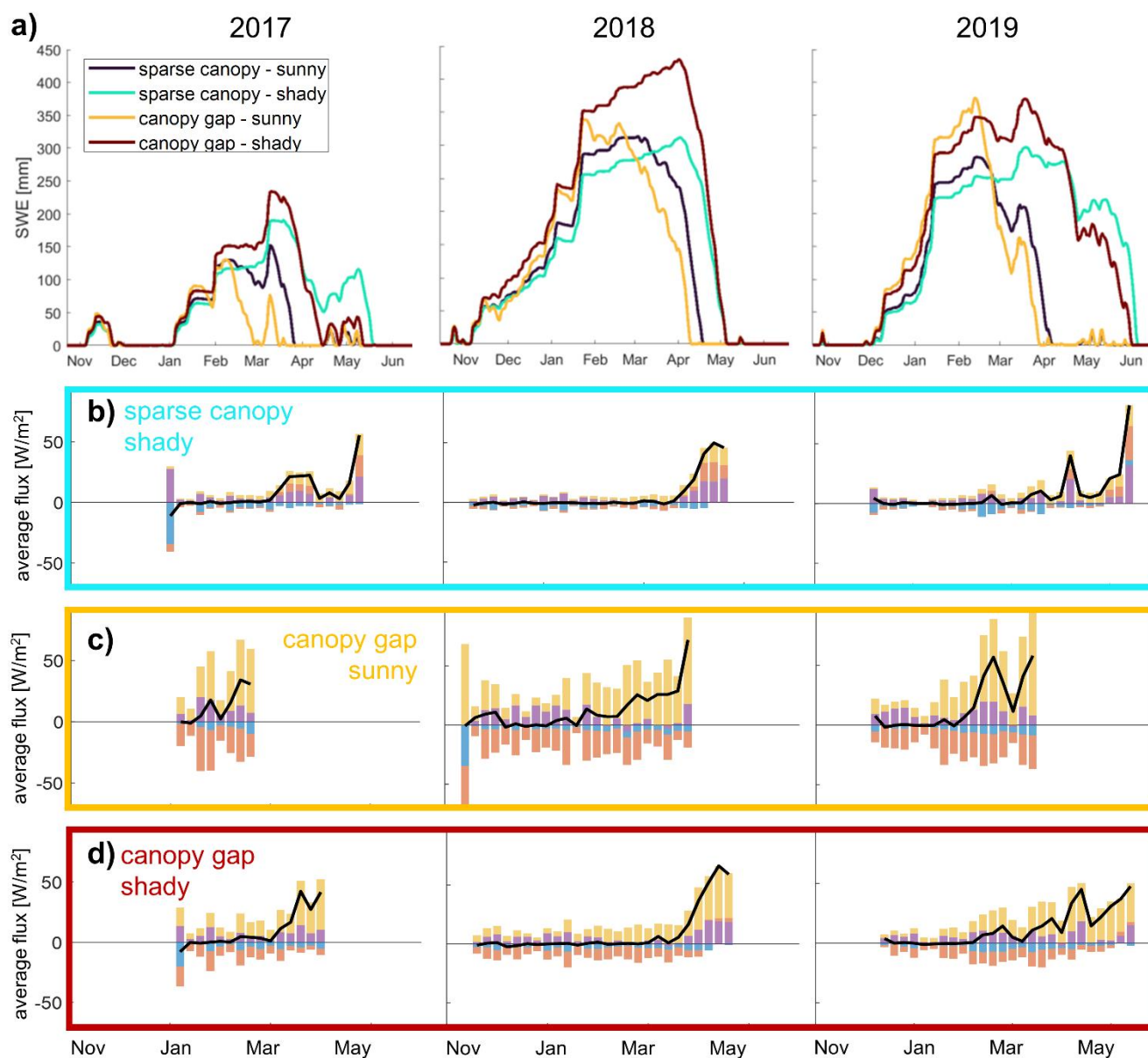
Figure 10: Impact of meteorological conditions illustrated by comparing three different WYs (columns), including (a) SWE evolution at four example points (locations see S3) and surface energy partitioning pathways at three of these, i.e. (b) a shady sparse canopy location, (c) a sunny canopy gap location, and (d) a shady canopy gap location.

425

Second, we note that the relative timing of snow disappearance between years can vary across the domain, based on the availability of melt energy over the course of the season (Figure 10a). Points that normally receive early-season shortwave irradiance (i.e., the dark blue and the yellow point) melt out later in WY 2018 compared to 2019 because less shortwave

irradiance is available in February (see strong positive shortwave contributions in Figure 10c). In contrast, points in shadier
430   locations (cyan and red) melt earlier in WY 2018 because of the consistently warmer and sunnier weather in spring
compared to 2019 (see earlier switch to both positive shortwave and longwave contributions in Figure 10b+d). The opposed
effect of these differences in meteorological conditions causes snow disappearance day of the four points to be much closer
in WY 2018 than in 2019. The overall melt-out patterns will thus vary between WYs, even if the dominating fluxes at each
specific location remain approximately consistent (Figure 10b-d).

4 Discussion

4.1 Process-level insights

Spatio-temporal snow cover dynamics and associated snow accumulation and melt patterns are a result of superimposed
processes that themselves vary as a function of both time-invariant physiographic features (vegetation, topography) and
time-varying meteorological conditions. While the phenological analysis of snow season descriptors presented in Sections
440   3.1-3.2 paints a complex picture of snow distribution patterns, the process-level analysis in Sections 3.3-3.5 allowed us to
attribute the processes that underly these patterns. The main takeaway from this work is that patterns of snow season
descriptors and their inter-seasonal consistency can only be explained by considering all three factors, canopy structure,
topography, and meteorology, as well as their interaction throughout the snow season.

Snow distribution patterns at any point in time arise from an interplay between accumulation and ablation patterns. For the
445   study site considered here, our analysis showed that snow cover dynamics result from the superposition of (1) a pattern that
is temporally static and dependent on canopy structure alone, with more snow where there is less canopy (i.e., accumulation
mostly controlled by interception) and (2) a time-varying pattern with complex dependencies on canopy structure, solar
position, weather, and topography, with an overall tendency for faster melt where there is less canopy (i.e., melt mostly
controlled by shortwave radiation). Depending on the relative strength of each of both signals, three regimes of snow cover
450   dynamics are principally possible:

R1.   Snow distribution can be described as function of canopy structure alone throughout the whole season. This is the
case when accumulation creates a strong signal, and melt patterns are too homogeneous or too weak to override this
signal, so that areas that accumulate less snow also melt out first.

R2.   Snow accumulation patterns can be described as a function of canopy structure during the accumulation period, but
455   those patterns will be overridden by melt patterns during the ablation period. Consequently, melt out date exhibits
no simple relationship with canopy structure.

R3.   Early-season melt inhibits formation of simple snow accumulation patterns, and snow distribution patterns remain
weakly correlated with canopy structure throughout the entire season.

Based on these regimes and using WY 2018 as an example, Figure 11 shows a conceptual subdivision of our model domain
460   into 4 zones. Zone A features no early-season melt and melt-out patterns that carry the imprint of local canopy cover; Zone B

is characterized by substantial early-season melt; Zones C and D largely lack early melt but exhibit fewer clear linkages between canopy cover and snow disappearance day. Note that Zones C and D are treated separately due to elevational differences. As a crosscheck, we computed the correlation coefficient between SWE and local canopy cover for each of the four zones separately in Figure 11d. As expected, Zone A (R1) features a strong negative correlation between SWE and local

465 canopy cover throughout the entire season; Zone D (R2) exhibits a similarly strong correlation at the beginning of the season which then degrades during ablation season; and Zone B (R3) a weaker correlation even early in the season, where each melt episode degrades and each interception event improves the correlation, until the ablation season causes the correlation to collapse more permanently. Zone C seems to show characteristics of R2 in 2018, but of R3 in 2016, which implies that the regime found at a specific location may not be consistent from year to year.

470
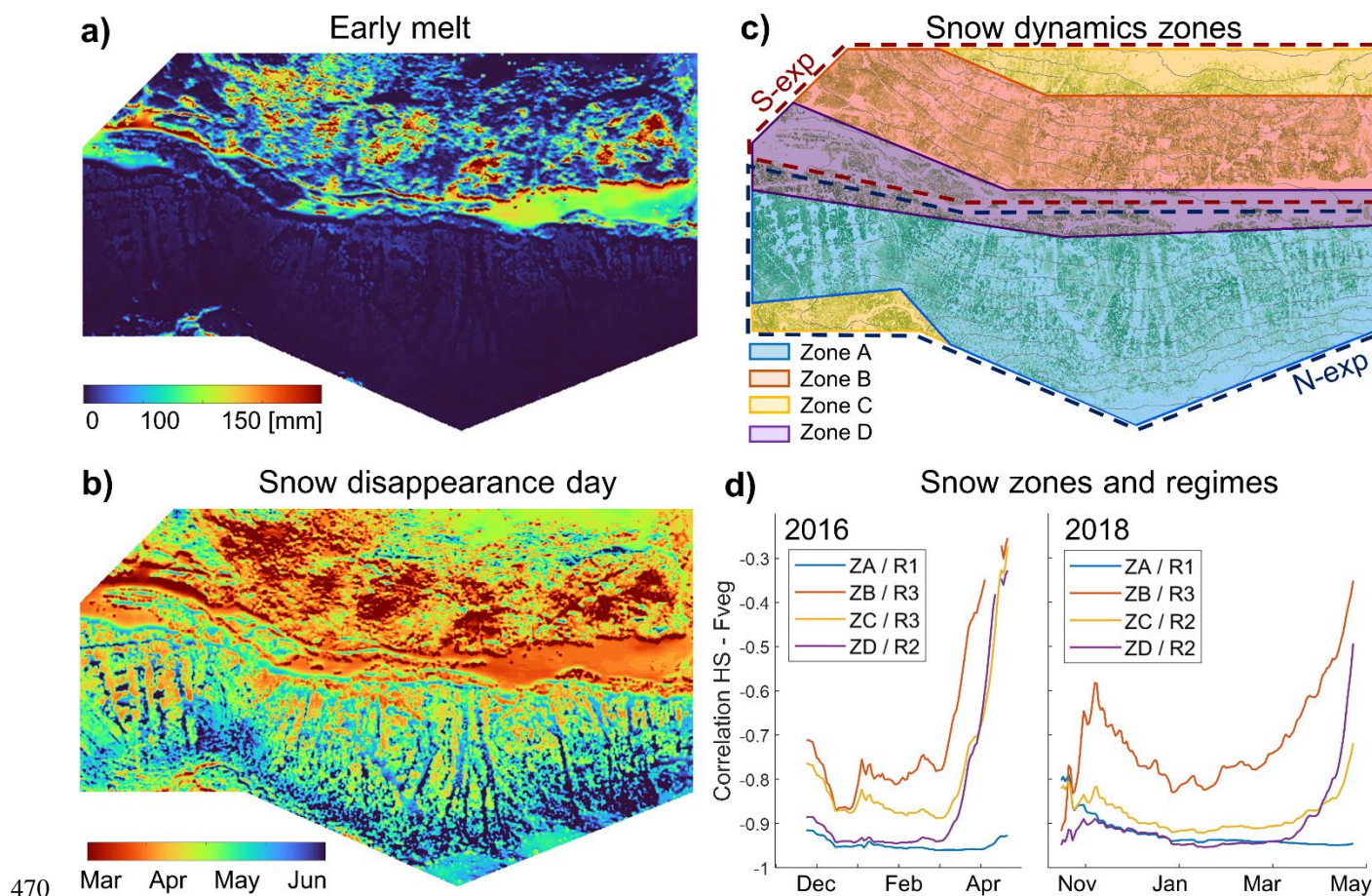
Figure 11: Conceptual subdivision of study domain into snow cover evolution regimes, the identification of which is based on maps of melt between mid-January and mid-March (a) and snow disappearance day (b) in WY 2018. Resulting zones (c) and evolution of the correlation coefficients between snow depth and vegetation cover fraction in these for WYs 2016 and 2018, resulting in the attribution to a specific regime (d).

475   The co-occurrence of different regimes across our study domain is a consequence of topography because early-season shortwave irradiance is a prerequisite for regime 3, while its absence is a prerequisite for regime 1. North-exposed slopes are prone to falling into regime 1, while south-exposed slopes tend to conform with regime 3. Regime 2 is less evident in our example, but most likely to be found in flat areas with large canopy gaps, where early-season melt is not expected but substantial melt energy gradients can evolve during ablation. The impact of inter-annual variability in meteorological

480   conditions can lead to the same locations hosting different regimes in different WYs, where differences result from either weaker accumulation patterns or variations in strength and timing of shortwave irradiance.

The categorization of snow cover dynamics into regimes provides a context to temporal snapshots of snow distribution patterns, such as those derived from singular LiDAR datasets. The temporal evolution of correlation coefficients (Figure 11d) corroborates findings from Koutantou et al. (2022), who used maps of modelled sub-canopy irradiance to explain why

485   snow distribution patterns exhibited different dependencies on canopy structure at their north- and south-exposed survey sites. A decay of the correlation between snow distribution and canopy structure between two LiDAR acquisitions in spring was also observed by Mazzotti et al. (2019a) for sites with less topographic variability. In general, our process-level insights explain why these correlations can vary between years and regimes, as shown in this study, and hence why different studies may have observed different and sometimes inconsistent dependencies between snow and canopy variables, depending on

490   when and where data were acquired (e.g. Safa et al., 2021; Currier and Lundquist, 2018).

4.2 Implications and applications

The process-level insights discussed in the previous section have important implications in a variety of contexts in which small-scale variability of forest snow cover dynamics is relevant. We elaborate on three such examples in the following.

Firstly, our findings indicate that strategies to account for sub-grid variability in coarser-resolution models that are intended

495   for application to sub-alpine environments need to account for variations in canopy structure, topography, and meteorology. The south-exposed slope in our model domain featured stronger variability and more complex patterns of snow cover descriptors than the north-exposed slope, with impacts on the evolution of fractional snow-covered area in grid cells that include such terrain. To our knowledge, sub-grid variability parametrizations that incorporate these effects are inexistent to date (Dickerson-Lange et al., 2015; Mazzotti et al., 2021; Schneider et al., 2020), but their development is a promising

500   avenue for further model improvement. Alternatively, recent studies have suggested tiling schemes based on fine-scale canopy structure as an approach to representing sub-grid variability (Broxton et al., 2021; Currier et al., 2022). Our findings indicate that tiling strategies could be further refined by additionally accounting for topography.

Secondly, our simulations evidence a strong complexity in eco-hydrologically relevant processes across a still relatively limited study domain. The large range of snow cover durations observed creates spatial variability in ground insulating

505   properties and soil temperatures. Snow water input to the ground also exhibits strong spatial heterogeneity due to variability in snow melt magnitudes and rates, with further influences on soil moisture evolution. As soil conditions control a wide range of biophysical processes (Neumann et al., 2019; Stark et al., 2020; Harpold, 2016), their spatial heterogeneity

potentially implies strong variability of habitat characteristics across relatively small spatial scales (Niittynen et al., 2018). It is also possible that the observed process variability affects ecologically relevant snow properties such as surface layer density (Boelman et al., 2019; Gilbert et al., 2017) or the formation of ice layers in the snowpack (Rasmus et al., 2018). This is an unexplored research topic to date, as resolving these internal snowpack processes would require a more sophisticated snow scheme than available in FSM2. Coupling of detailed canopy representation to snow physics models such as Crocus (Vionnet et al., 2012; Lafaysse et al., 2017) and SNOWPACK (Bartelt and Lehning, 2002; Lehning et al., 2002; Gouttevin et al., 2015) would hence be a prerequisite. Overall, our results advocate that small-scale landscape heterogeneity needs to be considered when addressing snow-related eco-hydrological questions in sub-alpine forested environments.

Lastly, process-level insights allow us to spatially and temporally extrapolate our findings. While it is known that forest snow cover dynamics differ across climates (Lundquist et al., 2013; Dickerson-Lange et al., 2021; Safa et al., 2021), the same underlying processes are active everywhere. The snow distribution patterns found in this study may thus not be directly transferrable to other climatic conditions, but improved understanding of how physiographic and meteorological factors interact with one another allows us to better predict where and when certain processes will prevail. Likewise, these insights enable improved prediction of how patterns may shift following environmental change. Our findings suggest, for instance, that canopy removal may have the opposite effect in different topographic locations, i.e., earlier and faster ablation on south-exposed slopes but longer snow retention in north-exposed ones. Warmer temperatures earlier in the season would alter the relative timing of shortwave vs. longwave-radiation driven melt, which would likely alter melt-out patterns on south-exposed slopes but only show minor impacts on north-exposed slopes. The use of hyper-resolution models in impact studies is still underexploited, but should be encouraged in the future, especially given that forest snowpacks in sub-alpine regions reside at climate-sensitive elevations (Schöner et al., 2019; Pepin et al., 2015), and forest structural change is widely and rapidly happening (Albrich et al., 2020; Goeking and Tarboton, 2020).

4.3 Assets, limitations, and outlook

Considerations in Sections 4.1 and 4.2 underline the assets of a process-based modelling approach in terms of its capabilities to resolve individual process dynamics. Additionally, modelling allowed us to obtain spatially and temporally continuous information, which is not feasible with today's observation technology. Most ALS-based snow datasets that cover large areas are available for only a few temporal snapshots (Safa et al., 2021; Currier and Lundquist, 2018; Harpold et al., 2014; Broxton et al., 2019), while existing attempts to acquire snow distribution time series are very limited in spatial extent and mostly cover one winter season only (Koutantou et al., 2022; Broxton and van Leeuwen, 2020). Process-level data that is both spatially and temporally explicit is even more scarce and extremely challenging to obtain (Moeser et al., 2015; Malle et al., 2019, 2021; Mazzotti et al., 2019b). Model application, in contrast, is only limited by the availability of driving meteorological data and surface datasets, and thus potentially applicable to extensive spatial and temporal domains.

Modelled process dynamics can only yield satisfactory estimates of reality if the model representations of the processes involved are sufficiently accurate. While models like FSM2 already enable tackling relevant research questions, the

modelling community should strive for continued improvement. On one hand, the representation of some processes, especially those involving snow in the canopy, could still be improved (Lundquist et al., 2021; Lumbrazo et al., 2022) and associated uncertainties should be evaluated systematically across the full range of canopy structure and topographic diversity of the application domains of interest. At hyper-resolutions, mass and energy exchange between neighbouring

545   locations becomes relevant (Schlögl et al., 2018), and lateral coupling would likely improve the representation of expanding snow-free areas in spring. Coupling to a soil or eco-hydrological model (Fatichi et al., 2012; Tague and Band, 2004) would further extend the potential applications of hyper-resolution forest snow schemes beyond just snow cover dynamics. Finally, a major challenge concerns the estimation of model parameters that are potentially variable in space. This approach was not pursued in this study but has been shown to considerably increase the benefits of calibration efforts (Wrzesien et al., 2022).

550   Approaches to automate model calibration across the full range of canopy structures and topographic settings may thus further improve the skill of models like FSM2.

In the longer term, combining hyper-resolution models and observations to leverage their complementary assets is likely the most promising avenue to advance our understanding of forest snow cover dynamics in complex terrain. Plausibility checks as presented in Section 2.3 are indispensable for the verification of model use cases, as well as for continued model

555   enhancement and refinement, and there is potential for improvement here as well. For instance, the use of RGB satellite data to validate melt out patterns (Section 2.3) is promising despite limited visibility of snow under the canopy. Automated algorithms to extract snow cover information from RGB imagery are not currently applicable to forested complex terrain (Deschamps-Berger et al., 2020; Gascoin et al., 2019), but would encourage the use of such datasets for this purpose. If respective workflows are continuously improved, enabling simulations and observations to be used in tandem and to benefit

560   from each other (e.g. through data assimilation approaches), hyper-resolution model applications at large temporal and spatial scales in the contexts discussed in Section 4.2 promise advances in eco-hydrological and land surface modelling research.

5 Conclusion

This study represents the first multi-year application of a hyper-resolution forest snow model capable of resolving tree-scale

565   processes within a sub-alpine valley, aimed at investigating how snow cover dynamics and the underlying processes are shaped by the interplay of (1) canopy structure, (2) terrain, and (3) meteorological conditions. The chosen approach yielded process-level insights that could not be obtained based on snow distribution datasets alone.

Our findings evidenced that all these three factors must be considered when attempting to explain spatio-temporal snow cover dynamics. Canopy structure exerts the primary control on accumulation patterns, yet the resulting snow distribution

570   can be disrupted by ablation patterns, which are primarily driven by the distribution of shortwave radiation. Because shortwave radiation exhibits complex canopy dependencies and tends to counteract accumulation patterns, it is the timing of radiation relative to the strength of the accumulation patterns that determines whether accumulation patterns persist until

melt-out, or whether they are overridden by more complex ablation patterns. Since amount and timing of shortwave irradiance are largely controlled by topography, south-exposed slopes are more prone to accumulation patterns being
575 superseded by ablation patterns even early in the season compared to north-exposed slopes, where accumulation patterns likely persist throughout melt-out. Finally, variability in meteorological conditions alters the relative strength of processes (accumulation, direct insolation, longwave driven melt) and can thus cause snow accumulation and melt pattern inconsistencies between years. This framework explains why snow distribution patterns in some areas exhibit a strong relationship with canopy structure, while they do not in other areas, and why this can change between years.

580 Process understanding gained from this work provides context to existing snow distribution datasets and a proof of concept for the continued development and application of hyper-resolution modelling approaches to forest-snow related research in complex terrain. Potential usages include questions that revolve around developing sub-grid variability parametrization in coarse-resolution models, exploring the eco-hydrological effects of the observed small-scale snow dynamics, and the application of hyper-resolution models in environmental change impact studies.

585 *Data and code availability.* The FSM2 model code is available on GitHub under https://github.com/GiuliaMazzotti/FSM2/tree/hyres_enhanced_canopy. Model input datasets are available on WSL's data repository EnviDat (doi:10.16904/envidat.338).

Author contributions. GM and TJ designed the study. CW did the radiation modelling and provided canopy structure input datasets for FSM2. LQ and BC contributed to the development of the model framework and the preparation of
590 meteorological input data. GM performed FSM2 simulations and analysed the results, with input from TJ. GM wrote the manuscript, with feedback from all authors.

Competing interests. The authors declare that they have no conflict of interests.

Acknowledgements. This study was partly funded by the WSL Institute for Snow and Avalanche Research SLF and by the Swiss Federal Office for the Environment (FOEN). Part of this work was carried out at the Centre des Études de la Neige
595 (MétéoFrance) under SNSF Postdoc.Mobility grant P500PN_202741. We would like to thank Kalliopi Koutantou for providing UAV-LiDAR data and for many informal chats during fieldwork, which sparked the idea for this research. We thank Christian Ginzler for giving us access to Planetscope data. We are grateful to Rebecca Mott and Jan Magnusson from the Operational Snow Hydrological Service at SLF for their support on matters related to the meteorological input and the model framework and to Richard Essery for his help with FSM2-related questions. We appreciated numerous scientific
600 discussions with Jessica Lundquist, Matthieu Lafaysse and Jari-Pekka Nousu while this work was taking shape.

References

Albrich, K., Rammer, W., and Seidl, R.: Climate change causes critical transitions and irreversible alterations of mountain forests, Global Change Biology, 26, 4013–4027, https://doi.org/10.1111/gcb.15118, 2020.

Barnhart, T. B., Molotch, N. P., Livneh, B., Harpold, A. A., Knowles, J. F., and Schneider, D.: Snowmelt rate dictates streamflow: Snowmelt Rate Dictates Streamflow, Geophys. Res. Lett., 43, 8006–8016, https://doi.org/10.1002/2016GL069690, 2016.

Bartelt, P. and Lehning, M.: A physical SNOWPACK model for the Swiss avalanche warning Part I: numerical model, Cold Regions Science and Technology, 23, 2002.

Bebi, P., Seidl, R., Motta, R., Fuhr, M., Firm, D., Krumm, F., Conedera, M., Ginzler, C., Wohlgemuth, T., and Kulakowski, D.: Changes of forest cover and disturbance regimes in the mountain forests of the Alps, For Ecol Manage, 388, 43–56, https://doi.org/10.1016/j.foreco.2016.10.028, 2017.

Boelman, N. T., Liston, G. E., Gurarie, E., Meddens, A. J. H., Mahoney, P. J., Kirchner, P. B., Bohrer, G., Brinkman, T. J., Cosgrove, C. L., Eitel, J. U. H., Hebblewhite, M., Kimball, J. S., LaPoint, S., Nolin, A. W., Pedersen, S. H., Prugh, L. R., Reinking, A. K., and Vierling, L. A.: Integrating snow science and wildlife ecology in Arctic-boreal North America, Environ. Res. Lett., 14, 010401, https://doi.org/10.1088/1748-9326/aaeec1, 2019.

Bormann, K. J., Brown, R. D., Derksen, C., and Painter, T. H.: Estimating snow-cover trends from space, Nature Climate Change, 8, 924–928, https://doi.org/10.1038/s41558-018-0318-3, 2018.

Broxton, P. D. and van Leeuwen, W. J. D.: Structure from Motion of Multi-Angle RPAS Imagery Complements Larger-Scale Airborne Lidar Data for Cost-Effective Snow Monitoring in Mountain Forests, Remote Sensing, 12, 2311, https://doi.org/10.3390/rs12142311, 2020.

Broxton, P. D., Harpold, A. A., Biederman, J. A., Troch, P. A., Molotch, N. P., and Brooks, P. D.: Quantifying the effects of vegetation structure on snow accumulation and ablation in mixed-conifer forests, Ecohydrol., 8, 1073–1094, https://doi.org/10.1002/eco.1565, 2015.

Broxton, P. D., Leeuwen, W. J. D., and Biederman, J. A.: Improving Snow Water Equivalent Maps With Machine Learning of Snow Survey and Lidar Measurements, Water Resour. Res., 55, 3739–3757, https://doi.org/10.1029/2018WR024146, 2019.

Broxton, P. D., Leeuwen, W. J. D., and Biederman, J. A.: Forest cover and topography regulate the thin, ephemeral snowpacks of the semiarid Southwest United States, Ecohydrology, 13, https://doi.org/10.1002/eco.2202, 2020.

Broxton, P. D., Moeser, C. D., and Harpold, A.: Accounting for Fine-Scale Forest Structure is Necessary to Model Snowpack Mass and Energy Budgets in Montane Forests, Water Resources Research, 57, e2021WR029716, https://doi.org/10.1029/2021WR029716, 2021.

Currier, W. R. and Lundquist, J. D.: Snow Depth Variability at the Forest Edge in Multiple Climates in the Western United States, Water Resour. Res., 54, 8756–8773, https://doi.org/10.1029/2018WR022553, 2018.

Currier, W. R., Sun, N., Wigmosta, M., Cristea, N., and Lundquist, J. D.: The impact of forest-controlled snow variability on late-season streamflow varies by climatic region and forest structure, Hydrological Processes, 36, e14614, https://doi.org/10.1002/hyp.14614, 2022.

Deschamps-Berger, C., Gascoin, S., Berthier, E., Deems, J., Gutmann, E., Dehecq, A., Shean, D., and Dumont, M.: Snow depth mapping from stereo satellite imagery in mountainous terrain: evaluation using airborne laser-scanning data, The Cryosphere, 14, 2925–2940, https://doi.org/10.5194/tc-14-2925-2020, 2020.

Dickerson-Lange, S. E., Lutz, J. A., Gersonde, R., Martin, K. A., Forsyth, J. E., and Lundquist, J. D.: Observations of distributed snow depth and snow duration within diverse forest structures in a maritime mountain watershed, Water Resour. Res., 51, 9353–9366, https://doi.org/10.1002/2015WR017873, 2015.

Dickerson-Lange, S. E., Vano, J. A., Gersonde, R., and Lundquist, J. D.: Ranking Forest Effects on Snow Storage: A Decision Tool for Forest Management, Water Resources Research, 57, e2020WR027926, https://doi.org/10.1029/2020WR027926, 2021.

Ellis, C. R., Pomeroy, J. W., Essery, R. L. H., and Link, T. E.: Effects of needleleaf forest cover on radiation and snowmelt dynamics in the Canadian Rocky Mountains, Can. J. For. Res., 41, 608–620, https://doi.org/10.1139/X10-227, 2011.

Essery, R.: A factorial snowpack model (FSM 1.0), Geoscientific Model Development, 8, 3867–3876, https://doi.org/10.5194/gmd-8-3867-2015, 2015.

Fatichi, S., Ivanov, V. Y., and Caporali, E.: A mechanistic ecohydrological model to investigate complex interactions in cold and warm water-controlled environments: 2. Spatiotemporal analyses, Journal of Advances in Modeling Earth Systems, 4, https://doi.org/10.1029/2011MS000087, 2012.

Gascoin, S., Grizonnet, M., Bouchet, M., Salgues, G., and Hagolle, O.: Theia Snow collection: high-resolution operational snow cover maps from Sentinel-2 and Landsat-8 data, Earth System Science Data, 11, 493–514, https://doi.org/10.5194/essd-11-493-2019, 2019.

Gilbert, S. L., Hundertmark, K. J., Person, D. K., Lindberg, M. S., and Boyce, M. S.: Behavioral plasticity in a variable environment: snow depth and habitat interactions drive deer movement in winter, Journal of Mammalogy, 98, 246–259, https://doi.org/10.1093/jmammal/gyw167, 2017.

Goeking, S. A. and Tarboton, D. G.: Forests and Water Yield: A Synthesis of Disturbance Effects on Streamflow and Snowpack in Western Coniferous Forests, Journal of Forestry, 118, 172–192, https://doi.org/10.1093/jofore/fvz069, 2020.

Gouttevin, I., Lehning, M., Jonas, T., Gustafsson, D., and Mölder, M.: A two-layer canopy model with thermal inertia for an improved snowpack energy balance below needleleaf forest (model SNOWPACK, version 3.2.1, revision 741), Geosci. Model Dev., 8, 2379–2398, https://doi.org/10.5194/gmd-8-2379-2015, 2015.

Griessinger, N., Schirmer, M., Helbig, N., Winstral, A., Michel, A., and Jonas, T.: Implications of observation-enhanced energy-balance snowmelt simulations for runoff modeling of Alpine catchments, Advances in Water Resources, 133, 103410, https://doi.org/10.1016/j.advwatres.2019.103410, 2019.

Harpold, A. A.: Diverging sensitivity of soil water stress to changing snowmelt timing in the Western U.S., Advances in Water Resources, 92, 116–129, https://doi.org/10.1016/j.advwatres.2016.03.017, 2016.

Harpold, A. A., Guo, Q., Molotch, N., Brooks, P. D., Bales, R., Fernandez-Diaz, J. C., Musselman, K. N., Swetnam, T. L., Kirchner, P., Meadows, M. W., Flanagan, J., and Lucas, R.: LiDAR-derived snowpack data sets from mixed conifer forests across the Western United States, Water Resour. Res., 50, 2749–2755, https://doi.org/10.1002/2013WR013935, 2014.

Harpold, A. A., Krogh, S. A., Kohler, M., Eckberg, D., Greenberg, J., Sterle, G., and Broxton, P. D.: Increasing the efficacy of forest thinning for snow using high-resolution modeling: A proof of concept in the Lake Tahoe Basin, California, USA, Ecohydrology, 13, https://doi.org/10.1002/eco.2203, 2020.

Jonas, T., Webster, C., Mazzotti, G., and Malle, J.: HPEval: A canopy shortwave radiation transmission model using high-resolution hemispherical images, Agricultural and Forest Meteorology, 284, 107903, https://doi.org/10.1016/j.agrformet.2020.107903, 2020.

Khosravipour, A., Skidmore, A. K., Isenburg, M., Wang, T., and Hussin, Y. A.: Generating Pit-free Canopy Height Models from Airborne Lidar, photogramm eng remote sensing, 80, 863–872, https://doi.org/10.14358/PERS.80.9.863, 2014.

Koutantou, K., Mazzotti, G., Brunner, P., Webster, C., and Jonas, T.: Exploring snow distribution dynamics in steep forested slopes with UAV-borne LiDAR, Cold Regions Science and Technology, 200, 103587, https://doi.org/10.1016/j.coldregions.2022.103587, 2022.

Krogh, S. A., Broxton, P. D., Manley, P. N., and Harpold, A. A.: Using Process Based Snow Modeling and Lidar to Predict the Effects of Forest Thinning on the Northern Sierra Nevada Snowpack, Front. For. Glob. Change, 3, 21, https://doi.org/10.3389/ffgc.2020.00021, 2020.

Lafaysse, M., Cluzet, B., Dumont, M., Lejeune, Y., Vionnet, V., and Morin, S.: A multiphysical ensemble system of numerical snow modelling, The Cryosphere, 11, 1173–1198, https://doi.org/10.5194/tc-11-1173-2017, 2017.

Lawler, R. R. and Link, T. E.: Quantification of incoming all-wave radiation in discontinuous forest canopies with application to snowmelt prediction, Hydrol. Process., 25, 3322–3331, https://doi.org/10.1002/hyp.8150, 2011.

Lehning, M., Bartelt, P., Brown, B., Fierz, C., and Satyawali, P.: A physical SNOWPACK model for the Swiss avalanche warning Part II. Snow microstructure, Cold Regions Science and Technology, 21, 2002.

Lumbrazo, C., Bennett, A., Currier, W. R., Nijssen, B., and Lundquist, J.: Evaluating Multiple Canopy-Snow Unloading Parameterizations in SUMMA With Time-Lapse Photography Characterized by Citizen Scientists, Water Resources Research, 58, e2021WR030852, https://doi.org/10.1029/2021WR030852, 2022.

Lundquist, J. D., Dickerson-Lange, S. E., Lutz, J. A., and Cristea, N. C.: Lower forest density enhances snow retention in regions with warmer winters: A global framework developed from plot-scale observations and modeling: Forests and Snow Retention, Water Resour. Res., 49, 6356–6370, https://doi.org/10.1002/wrcr.20504, 2013.

Lundquist, J. D., Dickerson-Lange, S., Gutmann, E., Jonas, T., Lumbrazo, C., and Reynolds, D.: Snow interception modelling: Isolated observations have led to many land surface models lacking appropriate temperature sensitivities, Hydrological Processes, 35, e14274, https://doi.org/10.1002/hyp.14274, 2021.

Malle, J., Rutter, N., Mazzotti, G., and Jonas, T.: Shading by Trees and Fractional Snow Cover Control the Subcanopy Radiation Budget, Journal of Geophysical Research: Atmospheres, 124, 3195–3207, https://doi.org/10.1029/2018JD029908, 2019.

Malle, J., Rutter, N., Webster, C., Mazzotti, G., Wake, L., and Jonas, T.: Effect of Forest Canopy Structure on Wintertime
705 Land Surface Albedo: Evaluating CLM5 Simulations With In-Situ Measurements, Journal of Geophysical Research: Atmospheres, 126, e2020JD034118, https://doi.org/10.1029/2020JD034118, 2021.

Manninen, T. and Jääskeläinen, E.: The Effect of Boreal Forest Canopy on Snow Covered Terrain Broadband Albedo, 21, 2018.

Manning, A. L., Harpold, A., and Csank, A.: Spruce Beetle Outbreak Increases Streamflow From Snow-Dominated Basins
710 in Southwest Colorado, USA, Water Resources Research, 58, e2021WR029964, https://doi.org/10.1029/2021WR029964, 2022.

Marty, C., Tilg, A.-M., and Jonas, T.: Recent Evidence of Large-Scale Receding Snow Water Equivalents in the European Alps, Journal of Hydrometeorology, 18, 1021–1031, https://doi.org/10.1175/JHM-D-16-0188.1, 2017.

Mazzotti, G., Currier, W. R., Deems, J. S., Pflug, J. M., Lundquist, J. D., and Jonas, T.: Revisiting Snow Cover Variability
715 and Canopy Structure Within Forest Stands: Insights From Airborne Lidar Data, Water Resources Research, 55, 6198–6216, https://doi.org/10.1029/2019WR024898, 2019a.

Mazzotti, G., Malle, J., Barr, S., and Jonas, T.: Spatially Continuous Characterization of Forest Canopy Structure and Subcanopy Irradiance Derived from Handheld Radiometer Surveys, Journal of Hydrometeorology, 20, 1417–1433, https://doi.org/10.1175/JHM-D-18-0158.1, 2019b.

720 Mazzotti, G., Essery, R., Webster, C., Malle, J., and Jonas, T.: Process-Level Evaluation of a Hyper-Resolution Forest Snow Model Using Distributed Multisensor Observations, Water Resources Research, 56, e2020WR027572, https://doi.org/10.1029/2020WR027572, 2020a.

Mazzotti, G., Essery, R., Moeser, C. D., and Jonas, T.: Resolving Small-Scale Forest Snow Patterns Using an Energy Balance Snow Model With a One-Layer Canopy, Water Resources Research, 56, e2019WR026129,
725 https://doi.org/10.1029/2019WR026129, 2020b.

Mazzotti, G., Webster, C., Essery, R., and Jonas, T.: Increasing the Physical Representation of Forest-Snow Processes in Coarse-Resolution Models: Lessons Learned From Upscaling Hyper-Resolution Simulations, Water Resources Research, 57, e2020WR029064, https://doi.org/10.1029/2020WR029064, 2021.

Moeser, C. D., Broxton, P. D., Harpold, A., and Robertson, A.: Estimating the Effects of Forest Structure Changes From
730 Wildfire on Snow Water Resources Under Varying Meteorological Conditions, Water Resources Research, 56, e2020WR027071, https://doi.org/10.1029/2020WR027071, 2020.

Moeser, D., Roubinek, J., Schleppi, P., Morsdorf, F., and Jonas, T.: Canopy closure, LAI and radiation transfer from airborne LiDAR synthetic images, Agricultural and Forest Meteorology, 197, 158–168, https://doi.org/10.1016/j.agrformet.2014.06.008, 2014.

735   Moeser, D., Stähli, M., and Jonas, T.: Improved snow interception modeling using canopy parameters derived from airborne L i DAR data, Water Resour. Res., 51, 5041–5059, https://doi.org/10.1002/2014WR016724, 2015.

Mote, P. W., Li, S., Lettenmaier, D. P., Xiao, M., and Engel, R.: Dramatic declines in snowpack in the western US, npj Climate and Atmospheric Science, 1, 1–6, https://doi.org/10.1038/s41612-018-0012-1, 2018.

Neumann, R. B., Moorberg, C. J., Lundquist, J. D., Turner, J. C., Waldrop, M. P., McFarland, J. W., Euskirchen, E. S.,
740   Edgar, C. W., and Turetsky, M. R.: Warming Effects of Spring Rainfall Increase Methane Emissions From Thawing Permafrost, Geophysical Research Letters, 46, 1393–1401, https://doi.org/10.1029/2018GL081274, 2019.

Niittynen, P., Heikkinen, R. K., and Luoto, M.: Snow cover is a neglected driver of Arctic biodiversity loss, Nature Climate Change, 8, 997–1001, https://doi.org/10.1038/s41558-018-0311-x, 2018.

Niittynen, P., Heikkinen, R. K., Aalto, J., Guisan, A., Kemppinen, J., and Luoto, M.: Fine-scale tundra vegetation patterns
745   are strongly related to winter thermal conditions, Nature Climate Change, 1–6, https://doi.org/10.1038/s41558-020-00916-4, 2020.

Notarnicola, C.: Hotspots of snow cover changes in global mountain regions over 2000–2018, Remote Sensing of Environment, 243, 111781, https://doi.org/10.1016/j.rse.2020.111781, 2020.

Painter, T. H., Berisford, D. F., Boardman, J. W., Bormann, K. J., Deems, J. S., Gehrke, F., Hedrick, A., Joyce, M., Laidlaw,
750   R., Marks, D., Mattmann, C., McGurk, B., Ramirez, P., Richardson, M., Skiles, S. M., Seidel, F. C., and Winstral, A.: The Airborne Snow Observatory: Fusion of scanning lidar, imaging spectrometer, and physically-based modeling for mapping snow water equivalent and snow albedo, Remote Sensing of Environment, 184, 139–152, https://doi.org/10.1016/j.rse.2016.06.018, 2016.

Pepin, N., Bradley, R. S., Diaz, H. F., Baraer, M., Caceres, E. B., Forsythe, N., Fowler, H., Greenwood, G., Hashmi, M. Z.,
755   Liu, X. D., Miller, J. R., Ning, L., Ohmura, A., Palazzi, E., Rangwala, I., Schöner, W., Severskiy, I., Shahgedanova, M., Wang, M. B., Williamson, S. N., Yang, D. Q., and Mountain Research Initiative EDW Working Group: Elevation-dependent warming in mountain regions of the world, Nature Climate Change, 5, 424–430, https://doi.org/10.1038/nclimate2563, 2015.

Pflug, J. M. and Lundquist, J. D.: Inferring Distributed Snow Depth by Leveraging Snow Pattern Repeatability: Investigation Using 47 Lidar Observations in the Tuolumne Watershed, Sierra Nevada, California, Water Resources Research, 56,
760   e2020WR027243, https://doi.org/10.1029/2020WR027243, 2020.

Rasmus, S., Kivinen, S., and Irannezhad, M.: Basal ice formation in snow cover in Northern Finland between 1948 and 2016, Environ. Res. Lett., 13, 114009, https://doi.org/10.1088/1748-9326/aae541, 2018.

Roth, T. R. and Nolin, A. W.: Characterizing Maritime Snow Canopy Interception in Forested Mountains, Water Resour. Res., 2018WR024089, https://doi.org/10.1029/2018WR024089, 2019.

765   Safa, H., Krogh, S. A., Greenberg, J., Kostadinov, T. S., and Harpold, A. A.: Unraveling the Controls on Snow Disappearance in Montane Conifer Forests Using Multi-Site Lidar, Water Resources Research, 57, e2020WR027522, https://doi.org/10.1029/2020WR027522, 2021.

Schlögl, S., Lehning, M., and Mott, R.: How Are Turbulent Sensible Heat Fluxes and Snow Melt Rates Affected by a Changing Snow Cover Fraction?, Frontiers in Earth Science, 6, 2018.

770 Schneider, D., Molotch, N. P., Deems, J. S., and Painter, T. H.: Analysis of topographic controls on depletion curves derived from airborne lidar snow depth data, Hydrology Research, 52, 253–265, https://doi.org/10.2166/nh.2020.267, 2020.

Schöner, W., Koch, R., Matulla, C., Marty, C., and Tilg, A.-M.: Spatiotemporal patterns of snow depth within the Swiss-Austrian Alps for the past half century (1961 to 2012) and linkages to climate change, International Journal of Climatology, 39, 1589–1603, https://doi.org/10.1002/joc.5902, 2019.

775 Seidl, R., Thom, D., Kautz, M., Martin-Benito, D., Peltoniemi, M., Vacchiano, G., Wild, J., Ascoli, D., Petr, M., Honkaniemi, J., Lexer, M. J., Trotsiuk, V., Mairota, P., Svoboda, M., Fabrika, M., Nagel, T. A., and Reyer, C. P. O.: Forest disturbances under climate change, Nature Climate Change, 7, 395–402, https://doi.org/10.1038/nclimate3303, 2017.

Seyednasrollah, B. and Kumar, M.: How Surface Radiation on Forested Snowpack Changes across a Latitudinal Gradient, Hydrology, 6, 62, https://doi.org/10.3390/hydrology6030062, 2019.

780 Siirila-Woodburn, E. R., Rhoades, A. M., Hatchett, B. J., Huning, L. S., Szinai, J., Tague, C., Nico, P. S., Feldman, D. R., Jones, A. D., Collins, W. D., and Kaatz, L.: A low-to-no snow future and its impacts on water resources in the western United States, Nat Rev Earth Environ, 2, 800–819, https://doi.org/10.1038/s43017-021-00219-y, 2021.

Stark, S., Martz, F., Ovaskainen, A., Vuosku, J., Männistö, M. K., and Rautio, P.: Ice-on-snow and compacted and absent snowpack exert contrasting effects on soil carbon cycling in a northern boreal forest, Soil Biology and Biochemistry, 150,
785 107983, https://doi.org/10.1016/j.soilbio.2020.107983, 2020.

Strasser, U., Warscher, M., and Liston, G. E.: Modeling Snow–Canopy Processes on an Idealized Mountain, Journal of Hydrometeorology, 12, 663–677, https://doi.org/10.1175/2011JHM1344.1, 2011.

Sturm, M., Goldstein, M. A., and Parr, C.: Water and life from snow: A trillion dollar science question, Water Resources Research, 53, 3534–3544, https://doi.org/10.1002/2017WR020840, 2017.

790 Tague, C. L. and Band, L. E.: RHESSys: Regional Hydro-Ecologic Simulation System—An Object-Oriented Approach to Spatially Distributed Modeling of Carbon, Water, and Nutrient Cycling, Earth Interactions, 8, 1–42, https://doi.org/10.1175/1087-3562(2004)8<1:RRHSSO>2.0.CO;2, 2004.

Vionnet, V., Brun, E., Morin, S., Boone, A., Faroux, S., Le Moigne, P., Martin, E., and Willemet, J.-M.: The detailed snowpack scheme Crocus and its implementation in SURFEX v7.2, Geosci. Model Dev., 5, 773–791,
795 https://doi.org/10.5194/gmd-5-773-2012, 2012.

Webster, C. and Jonas, T.: Influence of canopy shading and snow coverage on effective albedo in a snow-dominated evergreen needleleaf forest, Remote Sensing of Environment, 214, 48–58, https://doi.org/10.1016/j.rse.2018.05.023, 2018.

Webster, C., Rutter, N., Zahner, F., and Jonas, T.: Measurement of Incoming Radiation below Forest Canopies: A Comparison of Different Radiometer Configurations, Journal of Hydrometeorology, 17, 853–864,
800 https://doi.org/10.1175/JHM-D-15-0125.1, 2016.

Webster, C., Mazzotti, G., Essery, R., and Jonas, T.: Enhancing airborne LiDAR data for improved forest structure representation in shortwave transmission models, Remote Sensing of Environment, 249, 112017, https://doi.org/10.1016/j.rse.2020.112017, 2020.

Webster, C. S.: Measuring and modelling spatiotemporal longwave radiation dynamics in discontinuous forest environments, 2016.

Winstral, A., Jonas, T., and Helbig, N.: Statistical Downscaling of Gridded Wind Speed Data Using Local Topography, Journal of Hydrometeorology, 18, 335–348, https://doi.org/10.1175/JHM-D-16-0054.1, 2017.

Wood, E. F., Roundy, J. K., Troy, T. J., Beek, L. P. H. van, Bierkens, M. F. P., Blyth, E., Roo, A. de, Döll, P., Ek, M., Famiglietti, J., Gochis, D., Giesen, N. van de, Houser, P., Jaffé, P. R., Kollet, S., Lehner, B., Lettenmaier, D. P., Peters-Lidard, C., Sivapalan, M., Sheffield, J., Wade, A., and Whitehead, P.: Hyperresolution global land surface modeling: Meeting a grand challenge for monitoring Earth's terrestrial water, Water Resources Research, 47, https://doi.org/10.1029/2010WR010090, 2011.

Wrzesien, M. L., Kumar, S., Vuyovich, C., Gutmann, E. D., Kim, R. S., Forman, B. A., Durand, M., Raleigh, M. S., Webb, R., and Houser, P.: Development of a "Nature Run" for Observing System Simulation Experiments (OSSEs) for Snow Mission Development, Journal of Hydrometeorology, 23, 351–375, https://doi.org/10.1175/JHM-D-21-0071.1, 2022.

Zheng, Z., Ma, Q., Jin, S., Su, Y., Guo, Q., and Bales, R. C.: Canopy and Terrain Interactions Affecting Snowpack Spatial Patterns in the Sierra Nevada of California, Water Resour. Res., 55, 8721–8739, https://doi.org/10.1029/2018WR023758, 2019.